

# Conformational Effects on Excitonic Interactions in a Prototypical H-bonded Bichromophore: Bis(2-hydroxyphenyl)methane

Nathan R. Pillsbury, Christian W. Müller, and Timothy S. Zwier\*  
*Department of Chemistry, Purdue University, West Lafayette, Indiana 47907*

David F. Plusquellic\*  
*Biophysics Group, Physics Laboratory, National Institute of Standards and Technology, Gaithersburg, MD 20899-8443.*

## ABSTRACT

Laser induced fluorescence (LIF), single vibronic level fluorescence, UV holeburning, and fluorescence-dip infrared (FDIR) spectroscopy have been carried out on bis-(2-hydroxyphenyl)methane (2HDPM) in order to characterize the ground and first excited state vibronic spectroscopy of this model flexible bichromophore. These studies identified the presence of two conformational isomers. The FDIR spectra in the OH stretch region determine that conformer A is an OH $\cdots$ O H-bonded conformer, while conformer B is a doubly OH $\cdots$  $\pi$  H-bonded conformer with C<sub>2</sub> symmetry. High resolution, ultraviolet spectra ( $\sim$ 50 MHz resolution) of a series of vibronic bands of both conformers confirm and refine these assignments. The transition dipole moment direction in conformer A is consistent with electronic excitation that is primarily localized on the donor phenol ring. A tentative assignment of the S<sub>2</sub> origin is made to a set of transitions  $\sim$ 400 cm<sup>-1</sup> above S<sub>1</sub>. In conformer B, the TDM direction firmly establishes C<sub>2</sub> symmetry for the conformer in its S<sub>1</sub> state, and establishes the electronic excitation as delocalized over the two rings, as the lower member of an excitonic pair. The S<sub>2</sub> state has not been clearly identified in the spectrum. Based on CIS calculations, the S<sub>2</sub> state is postulated to be several times weaker than S<sub>1</sub>, making it difficult to identify, especially in the midst of overlap from vibronic bands due to conformer A. SVLF spectra show highly unusual vibronic intensity patterns, particularly in conformer B, which cannot be understood by simple harmonic Franck-Condon models, even in the presence of Duschinsky mixing. We postulate that these model flexible bichromophores have transition dipole moments that are extraordinarily sensitive to the distance and orientation of the two aromatic rings, highlighting the need to map out the transition dipole moment surface and its dependence on the (up to) five torsional and bending coordinates in order to understand the observations.

KEY WORDS: flexible bichromophore, OH $\cdots$  $\pi$  hydrogen bond, vibronic coupling, exciton splitting, transition dipole moment

\*Authors to whom correspondence should be addressed: [zwier@purdue.edu](mailto:zwier@purdue.edu);  
[david.plusquellic@nist.gov](mailto:david.plusquellic@nist.gov)

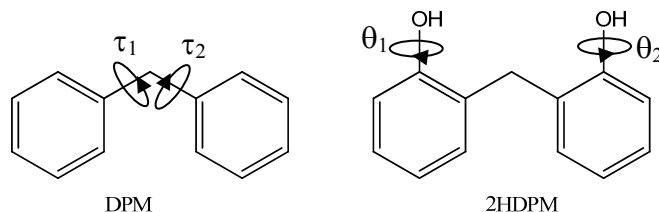
## I. INTRODUCTION

Conformational isomerization is a unimolecular reaction that involves hindered rotation about one or more single bonds. In simple cases, chemical intuition can guide the identification of conformational minima, and the reaction coordinate can be associated with motion along a well-defined single internal coordinate. However, as the size of the molecule and number of hindered rotations grows, isomerization evolves into a complicated motion occurring on a multi-dimensional potential energy surface. There has been considerable effort expended recently in studying the spectroscopy of flexible molecules large enough to support the formation of several conformational isomers.<sup>1-12</sup> In some cases, the spectroscopic characterization of these isomers has been followed by detailed studies of conformational isomerization initiated by laser excitation.<sup>13-17</sup>

Much recent work has focused attention on the conformation-specific spectroscopy of molecules with biological relevance, particularly on the molecular building blocks that make up proteins,<sup>8,12</sup> DNA,<sup>12</sup> and sugars,<sup>11</sup> or are representative of a particular biological function (e.g., neurotransmitters).<sup>1,10</sup> A complementary approach is to study conformational isomerization in a series of molecules chosen to be representatives of a particular type of potential energy surface. This approach was taken recently in a study of O-acetamidoethyl-N-acetyl-tyramine (OANAT), a prototypical doubly-substituted aromatic with two flexible side chains.<sup>18</sup>

The present paper describes the single-conformation spectroscopy of bis-(2-hydroxyphenyl)methane (2HDPM), whose structure is shown below. The ground state potential energy surface for 2HDPM supports minima that can be interconverted by hindered rotation about the two methylene C-phenyl C single bonds ( $\tau_1$ ,  $\tau_2$ ) and the two

C( $\phi$ )-O bonds ( $\theta_1, \theta_2$ ). This four-dimensional surface is rich in possibilities, because the two OH groups are in *ortho* positions on the two rings, placing them in close proximity to one another and to the other phenyl ring.



The two phenyl torsional coordinates present in 2HDPM are the two principal flexible coordinates in the prototypical molecule diphenylmethane (DPM). In that case, the relative orientation of the two phenyl rings can lead to various limiting structures in which the two rings take on T-shaped ( $\tau_1=0, \tau_2=90^\circ; \tau_1=90, \tau_2=0$ ,  $C_s$  symmetry), gable ( $\tau_1 = \tau_2=90^\circ$ ,  $C_{2v}$  symmetry), planar ( $\tau_1 = \tau_2 = 0$ ), or propeller-like geometries ( $\tau_1 = \tau_2 \neq 0, 90^\circ$ ,  $C_2$  symmetry). Based on high resolution data on the  $S_0$ - $S_1$  origin transition, DPM is known to adopt a propeller geometry with  $\tau_1 = \tau_2 = 55^\circ$  or  $125^\circ$ .<sup>19</sup> However, the striking prediction of calculations is that the  $S_0$  barriers to interconversion, which pass through gable or T-shaped transition states, are only about  $200 \text{ cm}^{-1}$  ( $2.5 \text{ kJ/mol}$ ) higher in energy than the minima.<sup>20</sup> To date, the spectroscopic results on DPM have not provided an experimental verification of this low barrier, because the observed torsional structure is harmonic over the range observed (up to  $120 \text{ cm}^{-1}$ ). Furthermore, the minima on the ground state surface of DPM are symmetry equivalent, and no evidence for tunneling between them has yet been observed in the rotational structure.<sup>19</sup>

The addition of two OH groups in forming 2HDPM from DPM increases the number of minima on the potential energy surface, modifies the barriers separating them, and provides a means by which the two rings can be distinguished from one another in

the case that conformers with  $C_1$  point group symmetry exist. A principal goal of the present work is to determine the conformational isomers present in 2HDPM and to characterize their infrared and ultraviolet spectral signatures in preparation for studies described in the adjoining paper that use population transfer methods<sup>21</sup> to map out the relative energies of the minima and the barriers separating them. As we shall see, two hydrogen-bonded conformers of 2HDPM are observed in the jet-cooled spectrum of the molecule. The ground state infrared spectra of the two conformers prove that one possesses a single  $\text{OH}\cdots\text{O}$  H-bond between the two OH groups, while the other possesses two equivalent  $\text{OH}\cdots\pi$  H-bonds between the OH group on one ring and the  $\pi$  cloud of the other.

Recently, Katsyuba et al. carried out a study of the infrared spectroscopy of 2HDPM in the liquid phase. The spectra so obtained could not be compared directly to calculated frequencies due to the strong intermolecular perturbations experienced by many of the bands (e.g., in the OH stretch region).<sup>22</sup> In order to get an accurate comparison, these types of calculations need to be compared to gas phase vibrational spectra. This paper provides these measurements.

Beyond characterizing key aspects of the four-dimensional potential energy surface for 2HDPM in the ground state, a second major thrust of the present work arises from the fact that 2HDPM is a flexible bichromophore. The two phenol rings in 2HDPM are identical ultraviolet chromophores that are chemically bonded to one another via a single methylene group, just as are the two phenyl rings in DPM. In that case, the  $S_1$ - $S_2$  energy separation is only  $123\text{ cm}^{-1}$ ,<sup>20</sup> and we anticipate the analogous two excited states of 2HDPM to also be in close proximity. As a result, the two surfaces and the vibronic

levels they support will be intimately intertwined with one another. The degree of localization or delocalization of the electronic excitation over the two rings and the separation between the two states should depend sensitively on the relative orientation of the two rings and on the asymmetry imposed on them by the OH groups and the H-bonds they form. The two conformers of 2HDPM provide an opportunity to characterize the excited state surface(s) by projecting onto them from two distinct regions of the ground state 4D surface, one associated with the OH $\cdots$ O conformer and the other the OH $\cdots$  $\pi$  bound conformer.

## II. EXPERIMENTAL METHODS

2HDPM was purchased from Sigma-Aldrich with a purity of 98% and used without further purification. A total pressure of 3.5 bar of helium was passed through a sample reservoir heated to 135°C. The gaseous sample was then injected into a vacuum chamber via a pulsed General Valve (Series 9) with a 0.8 mm orifice diameter. A roots pump backed by two mechanical pumps was used to evacuate the chamber to a running pressure of about 0.04 mbar (30 mTorr).

Laser induced fluorescence (LIF) and single vibronic level fluorescence (SVLF) spectra were obtained using a new chamber designed for both types of measurements. This chamber houses two 101.6 mm diameter spherical mirrors to increase fluorescence collection efficiency. The design is similar to others described previously.<sup>23-25</sup> An optics housing was built in such a way that the collected light could either be directed toward a photomultiplier tube (PMT) for LIF excitation scans or imaged onto the entrance slit of a monochromator for SVLF. A schematic diagram of the new chamber and optics housing

is given in **Figure 1**. The bottom spherical mirror (radius of curvature = -59.4 mm, focal length = 59.4 mm) collects the emission and focuses it back onto the optical axis of the chamber. The light then expands up to the top mirror and gets focused (along with the fluorescence that is collected by the top mirror (radius of curvature = -88.2 mm, focal length = 127.0 mm)) down through a small (~1 cm) hole in the bottom mirror. The collected light is collimated by a 50.8 mm diameter plano-convex lens (focal length = 50.8 mm.) inside the chamber before entering the optics housing. The housing is light-tight and made of half-inch polyvinylchloride (PVC). A sliding apparatus was built inside the housing to allow for a 45° turning mirror to either be pushed into or pulled out of the path of the collected fluorescence. When the mirror is pushed into the path of the fluorescence, the light is directed onto a PMT. LIF spectra were taken by collecting the total fluorescence signal as a function of excitation wavelength. Conversely, SVLF spectra were obtained by pulling the mirror out of the light path. This allows the fluorescence to be focused by another 50.8 mm diameter plano-convex lens (focal length = 180.3 mm) onto the entrance slit (typical slit width of 50-100  $\mu\text{m}$ ) of a 0.75 m monochromator (JY 750i, 2400 grooves/mm).<sup>58</sup> This lens is mounted in a modified vertical translation stage (Melles Griot, Dual-StableRod™), which can be adjusted by turning a knob on the bottom of the housing. The monochromator is fitted with a CCD camera (Andor series DU440BU2) at the exit port, which detects the dispersed emission. Two five-minute accumulations typically gave sufficient a signal-to-noise ratio (>100:1) for the SVLF scans. The excitation source was a Nd:YAG pumped dye laser system (Lambda Physik Scanmate 2E) with a typical UV power of ~0.1-0.3 mJ/pulse.

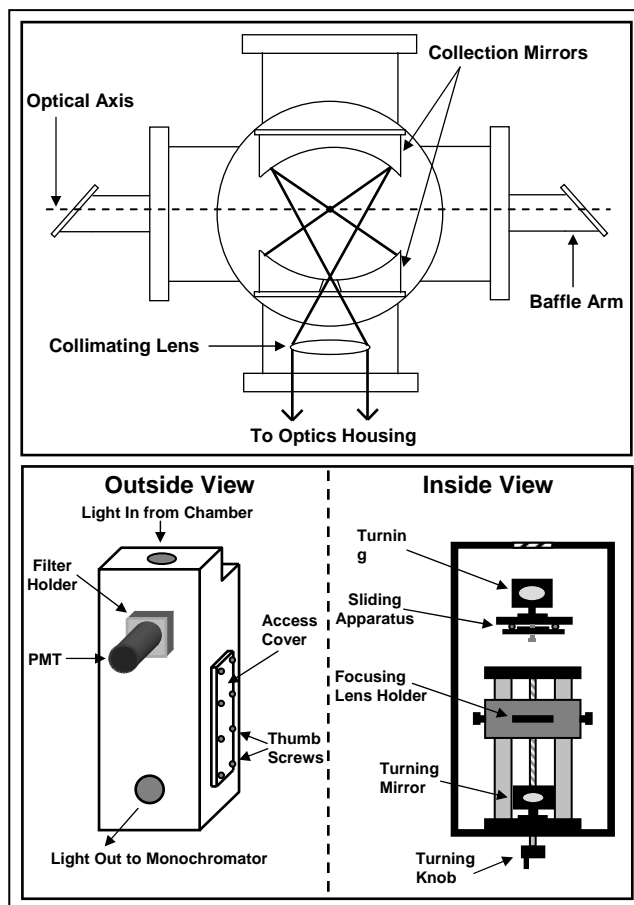


**Figure 1.** Top: Schematic of fluorescence vacuum chamber. Bottom: Schematic of optics housing.

A series of double resonance methods were employed to record conformation-specific infrared and ultraviolet spectra. All these methods used the active baseline subtraction mode of the gated integrator to record the difference in fluorescence signal from the probe laser between successive laser pulses, one with and one without the hole-burn laser present.

Conformation-specific ultraviolet spectra were recorded using ultraviolet hole-burning spectroscopy (UVHB). This technique involves fixing the wavelength of the HB laser (10 Hz) on a particular transition in the LIF spectrum and then scanning a probe laser, operating at 20 Hz, through the spectral region of interest. The probe laser is

delayed 50-200 ns from the HB laser (**Figure 2a**). When the wavelengths of the two lasers were fixed on transitions which share a common ground state, the probe laser signal was depleted by the absorption induced by the HB laser.

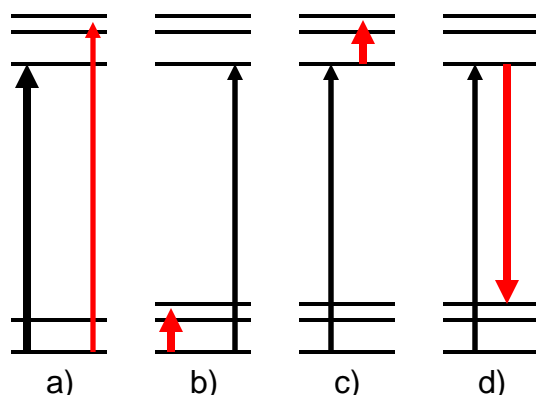


**Figure 2.** Energy level diagrams of various double resonance techniques used in this work: a) UVHB, b)  $S_0$  FDIR, c)  $S_1$  FDIR, and d) SEP. A thick arrow represents a 10 Hz laser while a thin arrow represents a 20 Hz laser. Red lines indicate the laser whose wavelength is tuned.

Ground and excited state infrared spectra of both conformations were acquired using fluorescence-dip infrared (FDIR) spectroscopy.<sup>26</sup> Infrared pulses ( $\sim 5$  mJ/pulse) were generated by a Nd:YAG pumped OPO/OPA system (LaserVision). For this experiment, the constant fluorescence signal from a particular transition in the LIF spectrum was monitored. Whenever an infrared pulse (10 Hz) resonant with a vibrational transition was introduced about 200 ns before the UV pulse (20 Hz), population in the ground state zero-point level was depleted (**Figure 2b**). Scanning the infrared parametric converter yielded the depletion signal which maps out the ground state infrared spectrum of the conformer of interest. To obtain the excited state spectra ( $S_1$  FDIRS), the infrared pulse

is introduced only a few nanoseconds after the UV excitation pulse (**Figure 2c**).

Depletion in the total fluorescence occurs when an infrared absorption of the excited state species is encountered.

Stimulated emission pumping (SEP) spectra were recorded by monitoring the total fluorescent signal from a particular transition (20 Hz) with the pump laser, while a second UV ‘dump’ laser ( $> 0.5$  mJ/pulse, 10 Hz) was scanned. The dump laser, delayed from the pump by 2-5 nsec, was scanned in wavelength, depleting the fluorescence by stimulating emission when the dump laser is resonant with Franck-Condon active transitions back to ground state vibrational levels (**Figure 2d**).

High resolution UV spectra of several vibronic transitions of both conformers were recorded using the apparatus at NIST, which has been described previously.<sup>25</sup> In that case, the sample was introduced into the chamber through a continuous quartz source with a 125  $\mu\text{m}$  orifice diameter. Argon was used as a backing gas at a pressure of 0.32 bar (240 Torr), and the 2HDPM sample was heated to about 190<sup>o</sup> C to obtain sufficient vapor pressure for the measurements. The laser system consisted of an Ar<sup>+</sup>-pumped (488 nm line) cw ring dye laser operating on Coumarin 521 laser dye<sup>27</sup> and generated  $\approx 500$  mW of laser light ( $\approx 1$  MHz) near 560 nm. Approximately 3 mW of the UV light at 280 nm was generated in an external resonant cavity containing a  $\beta$ -barium borate crystal. The molecular beam was skimmed and crossed at right angles with a slightly focused UV beam 18 cm downstream of the source. Laser induced fluorescence at the beam crossing was collected with 20 % efficiency using two spherical mirrors<sup>23,25</sup> and detected using a photomultiplier and computer interfaced photon counter. The Doppler limited resolution of the spectrometer using Ar carrier gas is 18( $\pm$ 1) MHz at 330 nm<sup>28</sup> and therefore is

expected to be 21( $\pm$ 1) MHz at 280 nm. Relative frequency calibration was performed using a HeNe stabilized reference cavity<sup>25,29</sup> and absolute frequencies were obtained using a wavemeter accurate to  $\pm 0.02 \text{ cm}^{-1}$ .

The rotationally resolved spectra were fit using a combination of techniques. Initial fits were obtained using a distributed parallel version of the Genetic Algorithm (GA) program similar to that described by Meerts and coworkers.<sup>30,31</sup> The algorithm was modified slightly to incorporate code to model inertial axis reorientation about any or all of the three inertial axes. The output files generated by this program were directly readable by the spectral fitting program, JB95.<sup>32,33</sup> Initial estimates of the GA parameters were determined from key features of the spectra. Because of the appearance of a prominent central *a*-type Q-branch, the initial GA runs included only *a*-type band character. Estimates of the ground state rotational constants were obtained from *ab initio* theory and reasonable ranges were placed on the parameter differences in  $S_1$  from the Q-branch shading and (B+C) level spacing. Once the rotational constants were sufficiently well determined, the hybrid band character was then fit.

The best fit rotational constants were determined by a linear least squares fitting procedure as implemented in the JB95 program. Calculations were performed using a standard Watson A-reduction Hamiltonian in representation  $I^r$ . Because of the large size of 2HDPM and resulting spectral congestion, transition frequencies were assigned in conjunction with refinements in the transition intensities. Using more restricted ranges ( $\pm 0.5 \%$ ) for the rotational constants in the GA program, the TDM components, axis reorientation angle(s), three temperature parameters<sup>34,35</sup>, and Lorentzian or Gaussian width were varied simultaneously. The simulated spectrum obtained from the average

parameters over several separate GA runs was generated and the rotational transitions were reassigned based on the line shape profiles. Satisfactory fits sometimes required first-order Watson distortion parameters in one or both electronic states. Finally, the intensity parameters were fit using a non-linear least squares fitting routine. The axis reorientation angle,  $\theta_{\mathbf{a}/\mathbf{b}\text{-reorient}}$ , represents the upper state frame rotation about the  $c$ -axis relative to the lower state with negative angles corresponding to a counter-clockwise rotation. Two other Euler angles were sometimes needed for fits of conformer A.

Calculations of the ground state conformational minima were performed at the DFT B3LYP<sup>36,37</sup>/6-31+G(d) and MP2<sup>38-43</sup>/6-311++G(d,p) levels of theory using Gaussian 03.<sup>39</sup> Harmonic vibrational frequencies (DFT) were obtained and utilized in the structural assignment process. Excited state optimizations were also performed using the CIS<sup>44</sup>/6-31G level of theory.

### III. RESULTS AND ANALYSIS

#### A. DFT Calculations

A search for conformational minima was performed by changing the positions of the hydroxyl groups and the orientations of the two rings and then optimizing the geometry using Gaussian 03 at the DFT B3LYP/6-31+G(d) level of theory. This search yielded two unique low-energy minima whose corresponding structures are shown in **Figure 3a,b**). The first structure has the hydroxyl group from one ring bonded to the hydroxyl group on the other ring in an OH $\cdots$ O H-bond (see **Figure 3a**). The second structure has  $C_2$  symmetry, with two identical H-bonds in which both hydroxyl groups are bonded to the  $\pi$ -cloud of the opposing ring (see **Figure 3b**). With ZPE corrections

included, the OH $\cdots$ O H-bonded structure is 3.03 kJ/mol more stable than the  $\pi$ -bound conformer at the DFT B3LYP/6-31+G(d) level but 3.18 kJ/mol less stable at the MP2/6-311++G(d,p) level. **Table 1** summarizes the calculated OH stretch frequencies and IR intensities and the predicted frequencies of the low-frequency vibrations (i.e. ring torsion, butterfly, etc.) calculated at the DFT B3LYP/6-31+G(d) level of theory for comparison with the experimental values determined in the following section.

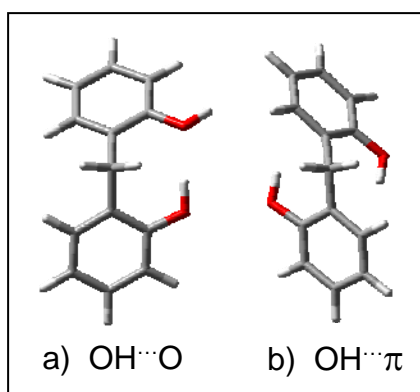


**Figure 3.** Lowest energy structures calculated at the DFT B3LYP/6-31+G\* level of theory.

**Table 1.** OH stretch and low-frequency vibrational frequencies of 2HDPM in the  $S_0$  state calculated at the DFT B3LYP/6-31+G(d) level of theory.

Conf.	Description**	Expt. Freq. (cm <sup>-1</sup> )	Calc. Freq.* (cm <sup>-1</sup> )	Calc. IR Int. (Km/mole)
A	Bound OH	3531	3519	496
	Com. Band	3558	-	
	Free OH	3657	3657	65
	T	28	27	
	$\beta$	79 or 83	55	
	$\bar{T}$	103 or 109	104	
	$\Omega$	125	149	
B	Bound OH	3560	3581	560
	T	37	41	
	$\bar{T}$	125/2 = 62.5	60	
	$\beta$	62	64	

\* scaled by 0.9726.

\*\*T is the symmetric torsion,  $\bar{T}$  is the antisymmetric torsion,  $\beta$  is the symmetric butterfly, and  $\Omega$  is the antisymmetric butterfly mode.

## B. Conformation-specific Spectroscopy

### 1. LIF Excitation and UVHB Spectra

The LIF spectrum of 2HDPM over the 35650-36320  $\text{cm}^{-1}$  region is shown in **Figure 4a**). This spectrum begins about 750  $\text{cm}^{-1}$  to the red of the *cis* o-cresol  $S_1 \leftarrow S_0$  origin transition<sup>45,46</sup> and is comprised of a dense set of vibronic transitions spread over several hundred wavenumbers. Since the observed spectrum can have contributions from more than one conformational isomer, UVHB spectroscopy was employed to determine the number of conformers present and their ultraviolet spectral signatures.

The UVHB spectra shown in **Figure 4b**) and **c**) were recorded with the hole-burn laser fixed at 35667 and 35834  $\text{cm}^{-1}$  respectively. All transitions in the spectrum can be attributed to two distinct conformational isomers, labeled 'A' and 'B'. Conformers A (2HDPM A) and B (2HDPM B) have  $S_1 \leftarrow S_0$  origin transitions at 35667 and 35811  $\text{cm}^{-1}$ , respectively. Long Franck-Condon (FC) progressions are evident in 2HDPM A, indicating a large geometry change upon electronic excitation. In the spectrum of 2HDPM A, all of the transitions in the first 300  $\text{cm}^{-1}$  can be accounted for using combinations of only two vibrational frequencies of 31 and 42  $\text{cm}^{-1}$ . By comparison, the spectrum of 2HDPM B is dominated by just three transitions, which are spaced from one another by 22  $\text{cm}^{-1}$ , suggesting a short vibronic progression in a 22  $\text{cm}^{-1}$  mode. These bands are interspersed in the midst of strong transitions from 2HDPM A, and careful selection of hole-burn wavelength was needed to record a clean UVHB spectrum. We will return later to assess the interpretation of the bands as a FC progression after the rest of the spectral characterization of 2HDPM B is complete.

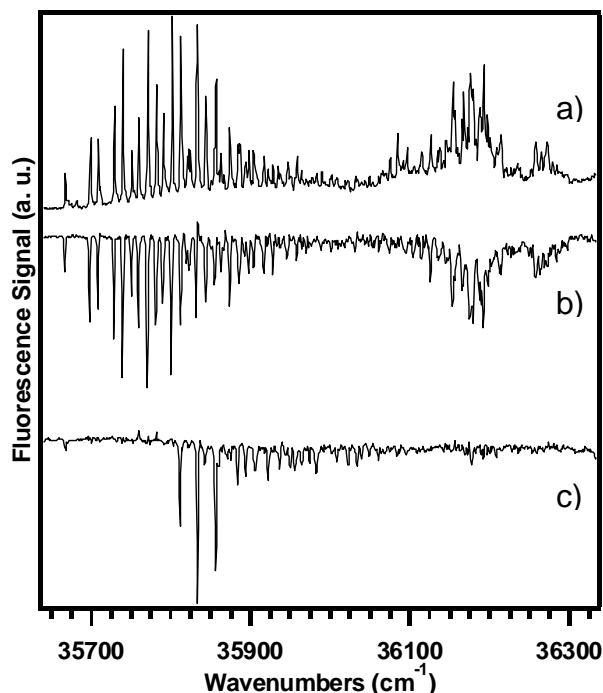


**Figure 4.** LIF (a) and UVHB spectra of conformers A (b) and B (c) of 2HDPM.

## 2. $S_0$ FDIR Spectra

Conformation-specific IR spectra in the OH stretch region were recorded using  $S_0$  FDIR spectroscopy. **Figure 5a)** shows the  $S_0$  FDIR spectrum of 2HDPM A in the region 3500-3700  $\text{cm}^{-1}$ . **Table 2** summarizes the observed OH stretch vibrational frequencies of the two conformers of 2HDPM, and compares them with the corresponding transitions in phenol monomer, phenol dimer, and the phenol-benzene complex. Two OH stretch fundamentals for 2HDPM A were observed at 3531 and 3657  $\text{cm}^{-1}$ . The latter transition is identical in frequency to the free OH stretch fundamental of gas phase phenol and the acceptor phenol in the phenol dimer.<sup>47</sup> Therefore, the transition at 3657  $\text{cm}^{-1}$  is assigned to a free OH stretch of one of the two OH groups.

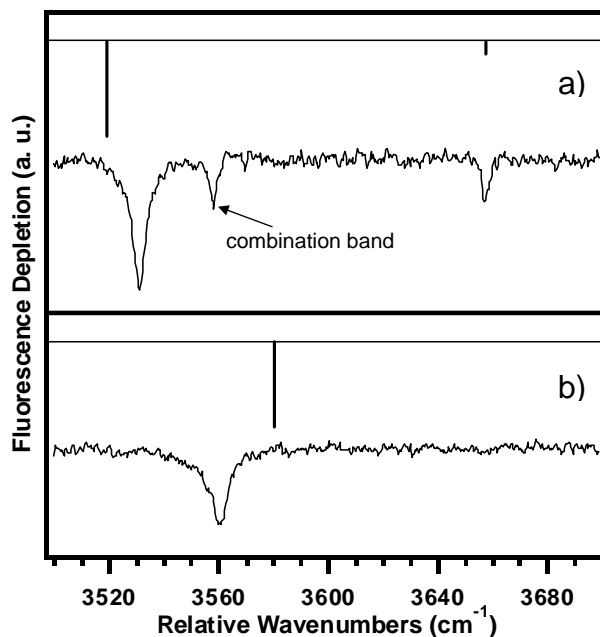


**Figure 5.**  $S_0$  FDIR spectra of 2HDPM A (a) and 2HDPM B (b). The stick spectra depict the OH stretch vibrational frequencies and infrared intensities calculated at the DFT B3LYP/6-31+G(d) level of theory.

**Table 2.** Comparison between the experimental OH stretch frequencies of 2HDPM, phenol, phenol dimer, and the phenol-benzene complex.

System	Bound OH $\cdots$ O ( $\text{cm}^{-1}$ )	Free OH ( $\text{cm}^{-1}$ )
Conformer A	3531	3657
Conformer B	3560	-
Phenol	-	3657 <sup>a</sup>
Phenol Dimer	3530 <sup>a</sup>	3654 <sup>a</sup>
Phenol-Benzene	3579	-

<sup>a</sup>Ref. 48.

Conversely, the band at  $3531\text{ cm}^{-1}$  can be attributed to a H-bonded OH stretch fundamental since it shows a characteristic shift to lower frequency, an increase in intensity, and an increase in breadth, all of which are signatures of a H-bonded OH group. In fact, the H-bonded OH stretch in 2HDPM A is within  $1\text{ cm}^{-1}$  of the donor phenol OH

in the phenol dimer ( $3530\text{ cm}^{-1}$ ).<sup>47</sup> This is interesting because the methylene group tethering the two rings in 2HDPM A constrains the inter-ring interaction, and therefore might be anticipated to result in formation a weaker H-bond.

The stick spectrum above the experimental spectrum in **Figure 5a**) displays the harmonic vibrational frequencies and infrared intensities computed at the DFT B3LYP/6-31+G(d) level of theory for the OH $\cdots$ O H-bonded structure shown in **Figure 3a**). The vibrational frequencies have all been scaled by 0.9726, a value chosen to match up the calculated and experimental free OH stretch fundamentals. The close correspondence between experiment and theory adds further weight to an assignment of conformer A as an OH $\cdots$ O H-bonded structure. We shall see shortly that the rotational structure from the high resolution ultraviolet scans also points to this same assignment.

There is also a weak band at  $3558\text{ cm}^{-1}$  in spectrum of 2HDPM A, which is not accounted for by the harmonic analysis. This transition is likely an OH stretch/inter-ring rock combination band, a point to which we will return after considering the dispersed fluorescence and SEP scans.

The  $S_0$  FDIR spectrum of 2HDPM B is shown in **Figure 5b**). Only one OH stretch fundamental was observed at  $3560\text{ cm}^{-1}$ . The presence of a single OH stretch in 2HDPM B is consistent with a symmetric structure in which one of the OH stretch fundamentals has zero intensity due to the cancellation of opposing dipoles. Furthermore, the observed band is located  $29\text{ cm}^{-1}$  higher in frequency than the H-bonded OH stretch of 2HDPM A, indicating that a slightly weaker hydrogen bond is involved. Both these features are consistent with the OH $\cdots$  $\pi$  structure shown in **Figure 3b**). The calculated stick spectrum for this  $\pi$ -bound structure is shown above the experimental

spectrum, using the same scale factor as in **Figure 5a**). Due to the  $C_2$  symmetry of this structure, the OH groups couple to one another to form in-phase and out-of-phase motions of the two OH bonds, as observed experimentally. In one case, the two add to one another, thereby enhancing its intensity, while the oscillating dipoles cancel in the out-of-phase fundamental. [Due to the  $C_2$  symmetry of this structure, the individual OH stretch vibrations linearly combine to form in-phase and out-of-phase motions of the two OH bonds. In the antisymmetric out-of-phase case, the two oscillating OH stretch dipole moments combine constructively, thus reinforcing each other, while they cancel in the symmetric in-phase fundamental.] As we shall see, the rotational structure from the ultraviolet high resolution scans (Section C1) confirms the 2HDPM B assignment.

### C. Spectroscopic Characterization of the Excited State

Having established the presence of two conformational isomers of 2HDPM and determined their H-bonded structure in the ground state, the experiments described in this section seek to characterize the excited states of these bichromophore conformers.

#### 1. High Resolution UV Spectra

High resolution UV spectra were taken of several prominent vibronic transitions in the LIF spectrum. The high resolution UV spectrum of the  $S_1 \leftarrow S_0$  origin transition of 2HDPM A is shown in **Figure 6a**). The top trace is the experimental spectrum and the bottom trace is the least-squares fit. A close-up view of a small portion of the spectrum is given **Figure 6b**) to highlight the quality of the fit. **Table 3** compares the experimental rotational constants of the  $S_0$  and  $S_1$  states for both conformers with the calculated constants from DFT B3LYP/6-31+G(d), MP2/6-311++G(d,p), and CIS/6-31G calculations. The good agreement between the ground state calculations and the

experiment lends considerable support to the assignments of the structures of both conformations based on the infrared spectroscopy. The CIS calculations are in reasonable agreement with the experimental excited state rotational constants ( $\pm 2$  to 4 %) and transition dipole moment (TDM) direction of 2HDPM A.

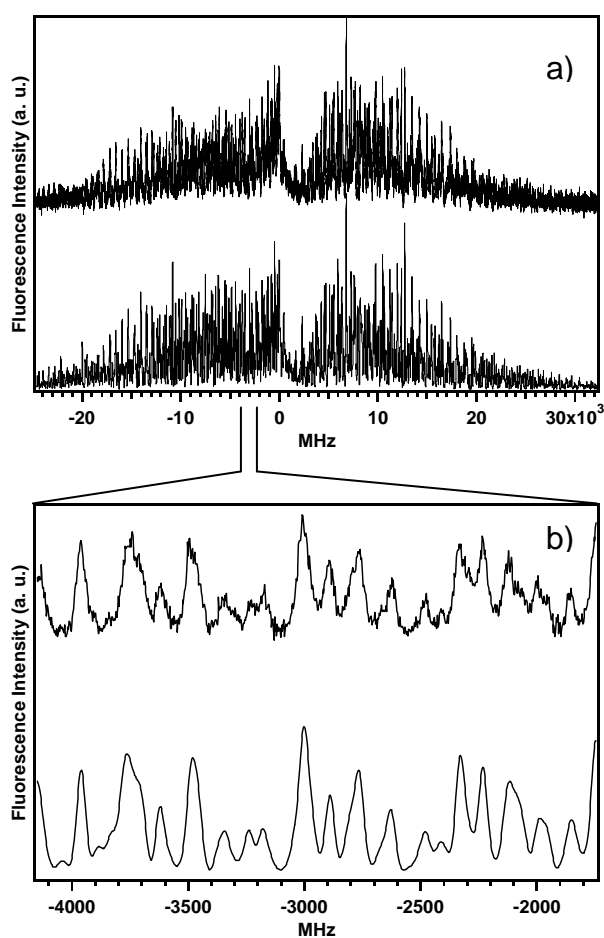


**Figure 6.** a) High resolution UV spectrum of the 2HDPM A origin transition. The top trace is the experimental spectrum and the bottom is the fit. b) Expanded view of a small spectral region to show the quality of the fit.

The full set of constants derived from the fit of the microwave spectrum,  $S_1 \leftarrow S_0$  origin,  $+31 \text{ cm}^{-1}$ , and  $+42 \text{ cm}^{-1}$  bands of 2HDPM A are included in **Table 4**. The table also includes the change in the rotational constants upon electronic excitation and magnitude of the axis reorientation that accompanies electronic excitation. The largest

change in rotational constant is along the A axis that passes through the two phenyl rings. A contraction of 40 MHz for rotation about this axis accompanies a strengthening of the H-bond upon electronic excitation. CIS calculations of 2HDPM A also predict this contraction of the two rings along the a-rotational axis by lowering the inter ring angle from 115 in  $S_0$  to 113 in  $S_1$ . The squares of the TDM components of the 2HDPM A origin band were found experimentally to be 82%:8%:10% along the a, b, and c-inertial axes respectively.

**Table 3.** Comparison between the experimental rotational constants of  $S_0$  and  $S_1$  states, change in rotational constants, and transition dipole moment projections with those calculated at the DFT B3LYP/6-31+G\*, MP2/6-311++G\*\*, and CIS/6-31G levels of theory.

Conformer A Origin					
	Expt.	DFT	MP2	HF*	CIS*
A / MHz	1158.2	1168.7	1129.6	1173.1	1158.6
B / MHz	412.5	404.6	418.7	409.6	412.2
C / MHz	348.1	336.9	346.6	338.1	341.1
$\Delta A$ / MHz	-39.5				-14.5
$\Delta B$ / MHz	9.5				2.6
$\Delta C$ / MHz	1.2				3.0
TDM a:b:c / %	82:8:10				87:5:8
Conformer B Origin					
	Expt.	DFT	MP2	HF*	CIS*
A / MHz	1326.2	1358.0	1302.6	1315.9	1308.8
B / MHz	402.4	389.7	412.1	396.1	393.2
C / MHz	368.8	360.7	376.9	354.6	351.5
$\Delta A$ / MHz	47.2				-7.1
$\Delta B$ / MHz	-16.1				-2.9
$\Delta C$ / MHz	-7.1				-3.1
TDM a:b:c / %	82:18:0				76:10:14

\*Hartree-Fock 6-31+G(d) calculations. The  $\Delta A$ ,  $\Delta B$ ,  $\Delta C$  values are calculated as  $A_{\text{CIS}} - A_{\text{HF}}$ , etc., since CIS is based on a HF description of the wave function.

The analogous best-fit parameters of all of the vibronic bands of 2HDPM A taken at high resolution are included in the supplementary material. (**Table S2**). This includes the +31, +42, and +73  $\text{cm}^{-1}$  bands, which are assigned as  $T^1_0$ ,  $\beta^1_0$ , and  $T^1_0\beta^1_0$  transitions

involving the two lowest wavenumber vibrations in the  $S_1$  state where T is the symmetric ring torsion and  $\beta$  is the symmetric butterfly motion of the two rings. The +145, +147 and +165  $\text{cm}^{-1}$  bands were recorded largely because of their close proximity to the 2HDPM B  $0_0^0$  and +22  $\text{cm}^{-1}$  bands.

**Table 4.** The constants derived from the fits to the indicated experimental bands using the JB95 fitting program. (See Tables S1 and S2 for a full set of constants).

	Origin A		+31 $\text{cm}^{-1}$ (A)		+42 $\text{cm}^{-1}$ (A)	
	$S_0^a$	$S_1$	$S_0^a$	$S_1$	$S_0^a$	$S_1$
$A'' / \Delta A / \text{MHz}$	1158.1642(3)	-39.550(3)	1158.1642(3)	-37.044(3)	1158.1642(3)	-39.597(6)
$B'' / \Delta B / \text{MHz}$	412.44646(3)	9.525(4)	412.44646(3)	+8.996(3)	412.44646(3)	+10.105(3)
$C'' / \Delta C / \text{MHz}$	348.12243(2)	1.176(5)	348.12243(2)	+0.896(1)	348.12243(2)	-1.802(2)
$\Delta I'' / \Delta \Delta I / \text{u}\cdot\text{\AA}^2$	-209.9546(2)	7.34(4)	-209.9546(2)	+8.01(1)	-209.9546(2)	+6.380(9)
Origin / $\text{cm}^{-1}$	35659.20(2)		35690.15(2) / 30.95(2)		35700.70(2) / 41.50(2)	
Band type / % <sup>b</sup>	82(2) <b>a</b> / 8(2) <b>b</b> / 10(2) <b>c</b>		81(2) <b>a</b> / 9(2) <b>b</b> / 10(2) <b>c</b>		81(2) <b>a</b> / 7(2) <b>b</b> / 12(2) <b>c</b>	
$\Delta \nu_{Lor} / \text{MHz}$ <sup>b,c</sup>	36(2)		35(2)		38(2)	
$T_1 / T_2 / \text{wt} / \text{K}$ <sup>b,d</sup>	2.6(2) / 10.8(5) / 0.20(5)		5.2(2) / 21.9(9) / 0.22(4)		5.2(2) / 23.0(9) / 0.21(2)	
$\varphi / \theta_{abc} / \chi / \sigma^b$	-6(2) / +3.26(5) / 4(2)		-1.2(8) / +3.304(6) / +1.7(8)		-3(2) / +3.234(8) / +5(2)	
	Origin B		+22 $\text{cm}^{-1}$ (B)		+44 $\text{cm}^{-1}$ (B)	
	$S_0^a$	$S_1$	$S_0^a$	$S_1$	$S_0^a$	$S_1$
$A'' / \Delta A / \text{MHz}$	1326.2890(1)	+47.319(10)	1326.2890(1)	+27.895(6)	1326.2890(1)	+22.761(4)
$B'' / \Delta B / \text{MHz}$	402.49068(5)	-16.077(9)	402.49068(5)	-11.812(3)	402.49068(5)	-10.937(1)
$C'' / \Delta C / \text{MHz}$	368.72377(8)	-7.140(7)	368.72377(8)	-5.653(3)	368.72377(8)	-5.229(1)
$\Delta I'' / \Delta \Delta I / \text{u}\cdot\text{\AA}^2$	-266.0597(3)	-12.05(3)	-266.0597(3)	-8.774(3)	-266.0597(3)	-8.927(5)
Origin / $\text{cm}^{-1}$	35802.94(2)		35825.67(2) / +22.73(2)		35848.06(2) / +45.12(2)	
Band type / % <sup>b</sup>	82(4) <b>a</b> / 18(4) <b>b</b>		79(4) <b>a</b> / 21(4) <b>b</b>		91(2) <b>a</b> / 9(4) <b>b</b>	
$\Delta \nu_{Lor} / \text{MHz}$ <sup>b,c</sup>	58(2)		59(2)		42(2)	
$T_1 / T_2 / \text{wt} / \text{K}$ <sup>b,d</sup>	2.8(1) / 8.7(4) / 0.31(8)		3.1(1) / 9.4(2) / 0.31(4)		3.0(1) / 8.0(2) / 0.31(4)	
$\theta_{ab} / \text{reorient} / \sigma^b$	+0.49(5)		+0.24		-0.05(4)	

<sup>a</sup>Ground state constants are based on fits of the microwave spectra and given in Table S1.

<sup>b</sup>Band type components, Lorentzian widths, temperatures and  $S_1$  state Euler angle reorientation angles (+ = ccw about c-axis) determined using genetic algorithms.

<sup>c</sup>Voigt lineshape fits include a fixed 21.3 MHz Gaussian component (FWHM) of the instrument.

<sup>d</sup>Based on a two-temperature model.<sup>34,48</sup>

**Table 5.** The set of vibration-rotation coupling constants associated with the +31, +42, and +147  $\text{cm}^{-1}$  excited state vibrations of 2HDPM A.

vibration ( $\text{cm}^{-1}$ )	$-\alpha_A$ (MHz)	$-\alpha_B$ (MHz)	$-\alpha_C$ (MHz)
+31	+2.479±0.056	-0.521±0.013	-0.282±0.015
+42	-0.045±0.055	+0.582±0.021	-2.970±0.015
+147	+2.665±0.536	-0.694±0.032	-0.355±0.030

**Figure 7** presents a graph of the changes in rotational constants ( $\Delta A$ ,  $\Delta B$ ) upon electronic excitation associated with each of the vibronic bands of conformer A recorded

at high resolution. As the lines joining these points indicate, the vibronic bands have changes in rotational constants that vary linearly with the assigned ( $v_T, v_\beta$ ) quantum-number make-up of the upper state, as is expected for the vibrational dependence of the effective rotational constants,  $A_v \equiv B_v^{(a)}$ ,  $B_v \equiv B_v^{(b)}$ , and  $C_v \equiv B_v^{(c)}$  in the quartic approximation.<sup>49,50</sup> In this approximation the effective rotational constant  $B_v$ , e. g., is linearly related to its pertinent vibrational-rotational interaction constants  $\alpha_r^B$  according to

$$B_v^{(b)} = B_v = B_e - \sum_{r=1}^{3N-6} \alpha_r^B \left( v_r + \frac{1}{2} \right)$$

Thus, the observed linear relationships between  $v_r$  and  $A_v$ ,  $B_v$ , and  $C_v$  can be used to obtain a set of vibrational-rotational interaction constants  $\alpha_r^\zeta$  ( $\zeta=A, B$ , and  $C$ ) associated with each vibrational mode  $r$ . These values are included in **Table 5**.

In order to see whether these vibration-rotation coupling constants had a clear association with the nature of the excited state vibration, we calculated the vibration-rotation interaction constants for the three lowest-frequency excited state vibrations from first-principles, for comparison with experiment. Contributions to  $\alpha_r^\zeta$  arise from the normal mode inertial-derivative, Coriolis effects, and anharmonicity. Details of this calculation are included in the **Supplementary Material**.

Vibration-rotation constants calculated for the three lowest frequency excited state vibrations of 2HDPM A using CIS/6-31G(d) calculation matched experiment poorly, and therefore cannot be used to check the form of the normal modes in the excited state, as we had hoped. Nevertheless, experimental excited state vibration-rotation constants with accuracies like those derived from the present fits present a

challenge to future computational studies seeking spectroscopic accuracy in excited electronic states.

As **Figure 7** bears out, the  $+147\text{ cm}^{-1}$  transition does not fall into the progressions involving  $\nu_T$  and  $\nu_\beta$ . This transition is a weak transition just to the blue of the 2HDPM B origin, which is partially overlapped with it. The unique changes in rotational constants associated with this band argue for its assignment to a new vibration. Based on the calculations (**Table 1**), a likely assignment for the band is  $\Omega^1_0$ , the out-of-phase butterfly motion of the two rings, with a calculated frequency of  $149\text{ cm}^{-1}$  in  $S_0$  and  $132\text{ cm}^{-1}$  in  $S_1$ .

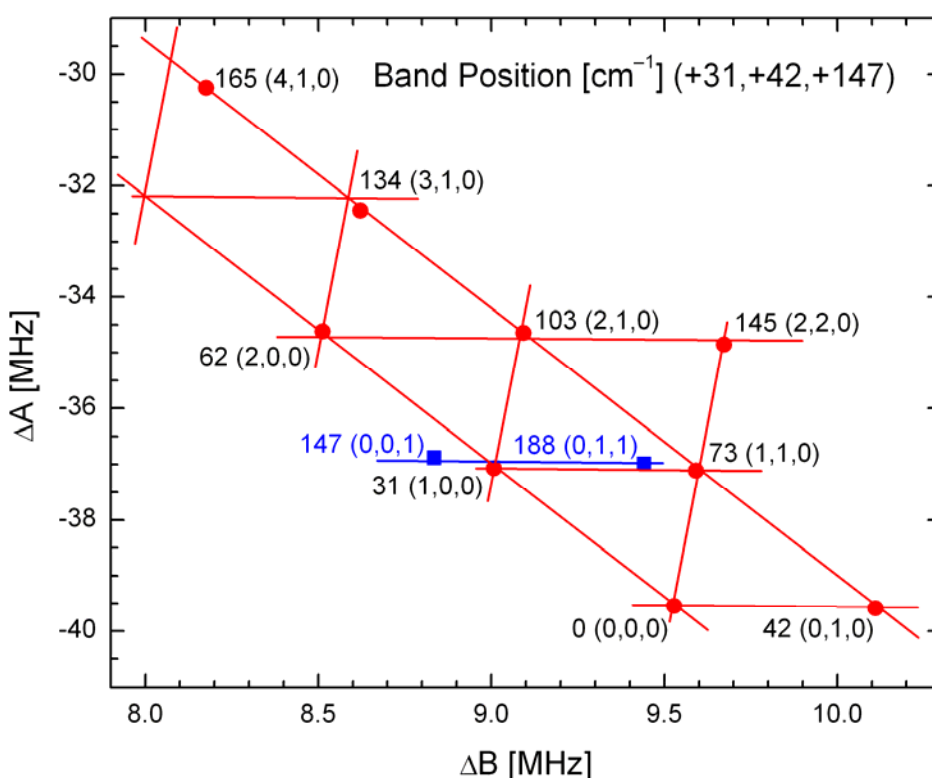


**Figure 7.** Plot of the change in rotational constants ( $\Delta A$  vs.  $\Delta B$ ) upon excitation to the indicated vibrational levels in the first excited state of 2HDPM(A). The labels indicate the peak position relative to the  $S_1$  origin (in  $\text{cm}^{-1}$ ) and the quantum number labeling in the modes with frequencies 31, 42, and  $147\text{ cm}^{-1}$  ( $\nu(+31\text{ cm}^{-1})$ ,  $\nu(+42\text{ cm}^{-1})$ ,  $\nu(+147\text{ cm}^{-1})$ ). Lines drawn are parallels (rather than fits to the data points), demonstrating the linearity in  $\Delta A$ ,  $\Delta B$  with quantum number. Note, however, the shift away from linearity in the high quantum number transitions at 134 and  $165\text{ cm}^{-1}$ .

**Figure 8a)** presents the rotational band structure for the  $+22\text{ cm}^{-1}$  transition of 2HDPM B. This band was free from overlap from 2HDPM vibronic bands and therefore its rotational structure was recorded and analyzed first. The fit to the spectrum is shown below the experimental trace in **Figure 8a)**. In order to illustrate the quality of the fit, as before, a 3 GHz section of the band is shown in **Figure 8b)** together with its corresponding fit. This band has a strong Q-branch indicating a TDM direction primarily along the a-rotational axis. According to the fit, the  $+22\text{ cm}^{-1}$  band is an a/b-hybrid band

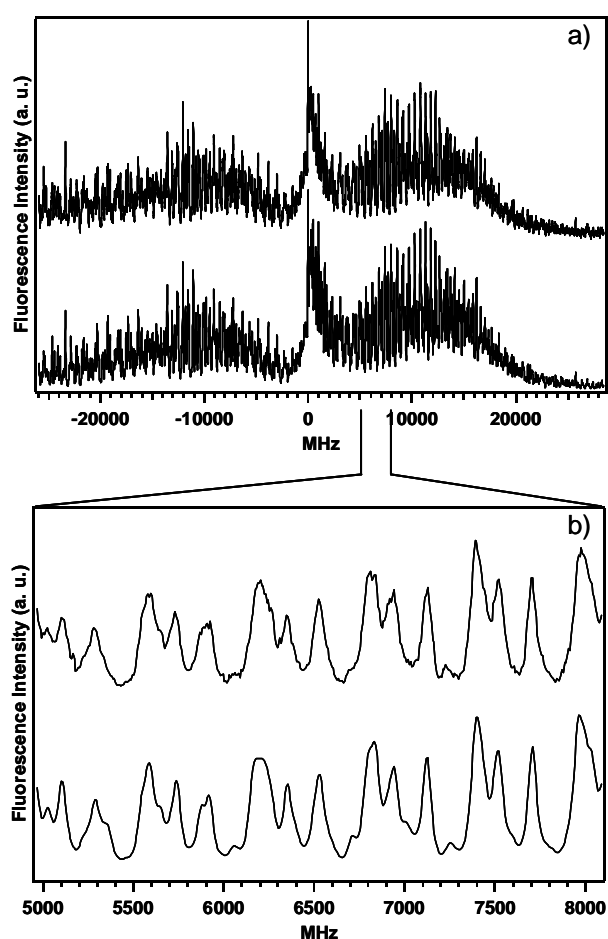


**Figure 8.** a): High resolution UV spectrum of the 2HDPM B  $+22\text{ cm}^{-1}$  transition. The top trace is the experimental spectrum and the bottom is the fit. b): Blow-up of a small spectral region to show the quality of the fit.

(79% a:21% b:0% c). Based on the infrared spectroscopy, we have already assigned 2HDPM B as a  $C_2$  symmetry doubly  $\pi$  H-bonded structure. The close correspondence between calculated and observed rotational constants and the small geometry change upon electronic excitation argue for retention of the  $C_2$  geometry by the excited state conformer. The direction of the TDM is also consistent with this deduction. It can be shown that in a bichromophore with  $C_2$  symmetry (e.g. DPM),<sup>20</sup> one excitonic state will have a TDM parallel to the  $C_2$  axis, while the TDM of the other will be in the plane perpendicular to the  $C_2$  axis. For 2HDPM B, the a-axis is down the long axis of the molecule through the phenol rings, and the c-axis (which is coincident with the “ $C_2$ ” axis) goes up through the methylene group from the center of mass. Therefore, if the excitation was totally delocalized, the TDM direction would either be 100% ‘c’ or a mixture of ‘a’ and ‘b’. The experimental observation of an a:b hybrid type band is thus consistent with retention of the  $C_2$  symmetry in the  $S_1$  state, with electronic excitation delocalized over both rings. We will return to this point in more detail in the discussion section.

Once a fit of the  $+22\text{ cm}^{-1}$  band of 2HDPM B was achieved, it could be used as a starting point for fitting the 2HDPM B origin and  $+44\text{ cm}^{-1}$  bands. The results of those fits are also included in **Table 4**. An interesting aspect of these fits is the large swing in TDM direction between the three bands, with the origin at 82% a:18% b, the  $+22\text{ cm}^{-1}$  band at 79% a:21% b, and the  $+44\text{ cm}^{-1}$  band at 91% a:9% b. By comparison, the TDM directions of the vibronic bands of 2HDPM A change by no more than 1% in ‘a’ character with up to  $165\text{ cm}^{-1}$  of vibrational excitation.

The changes in rotational constants which accompany electronic excitation of 2HDPM B (**Table 4**) are opposite to those in 2HDPM A. While the OH $\cdots$ O conformer has a negative  $\Delta A$  and positive  $\Delta B$ , the origin of the  $\pi$  bound conformer shows an increase in  $\Delta A$  by 47 MHz, while  $\Delta B$  and  $\Delta C$  decrease. This increase in  $\Delta A$  is consistent with a strengthening of the OH $\cdots$  $\pi$  H-bonds in 2HDPM B that rotates the oxygen atoms closer towards the inter-ring axis (the 'a' inertial axis). Furthermore, the +22 cm $^{-1}$  and +44 cm $^{-1}$  bands of 2HDPM B show changes in rotational constants ( $\Delta A=28$  MHz,  $\Delta B= -12$  MHz,  $\Delta C= -5$  MHz) that are about two-thirds the size of those for the 2HDPM B origin ( $\Delta A=+47$  MHz,  $\Delta B=-16$  MHz, and  $\Delta C=-7$  MHz). More importantly, while the frequency spacings of +22 and +44 cm $^{-1}$  suggest that these bands form a Franck-Condon progression in a 22 cm $^{-1}$  vibration, the changes of the rotational constants,  $\Delta A$ ,  $\Delta B$  and  $\Delta C$ , for these bands do not show the same linearity just discussed for the progressions in T and  $\beta$  of 2HDPM A. This casts some doubt on that interpretation. We will return to consider the anomalous aspects of these bands in more detail after presenting the SVLF spectra (Sec. D).

## 2. S<sub>1</sub> FDIR Spectra

Excited state FDIR spectra of the two conformers in the OH stretch region were also recorded for their S<sub>1</sub> $\leftarrow$ S<sub>0</sub> origins and a series of vibronic bands built off of these origins. This allowed us to observe the effect of electronic excitation on the OH stretch infrared spectrum, and test the influence of the excitation of low-frequency vibrations on the OH stretch transitions. These measurements were made possible because the S<sub>1</sub> lifetimes of the bands were sufficiently long that the nanosecond IR laser could deplete the fluorescence on a timescale shorter than the S<sub>1</sub> lifetime. Because the S<sub>1</sub> FDIR spectra

(and SVLF spectra that follow) were taken following excitation of a series of vibronic transitions, **Figure 9a** presents the hole-burning spectrum of 2HDPM A with the vibronic levels of interest labeled.

The  $S_1$  FDIR spectra of 2HDPM A are shown in **Figure 9b**). The dotted lines indicate the positions of the bound and free OH stretch transitions in the ground electronic state. While the free OH stretch fundamental remains very near its value in the ground state, the H-bonded OH stretch in the  $S_1$  state appears at  $3344\text{ cm}^{-1}$ , shifted down by an additional  $186\text{ cm}^{-1}$  from its value in the ground state. This large additional shift reflects a considerable strengthening of the  $\text{OH}\cdots\text{O}$  H-bond upon electronic excitation, much as it does in phenol dimer<sup>47</sup> in which the phenol molecule acts as H-bond donor. This provides convincing evidence that the electronic excitation is localized on the donor ring in the  $S_1$  state

Furthermore, the spectrum shows only very minor changes when the infrared spectrum is taken out of excited state levels carrying one or more quanta of torsional excitation. The spectrum in the bottom trace is taken from a band  $176\text{ cm}^{-1}$  above the  $S_1$  origin. Here, there is evidence for a slight weakening of the  $\text{OH}\cdots\text{O}$  H-bond with a shift of  $7\text{ cm}^{-1}$  to higher frequency relative to the origin spectrum. The splitting observed is a likely consequence of anharmonic coupling contributing to an excited state vibronic level of mixed character.

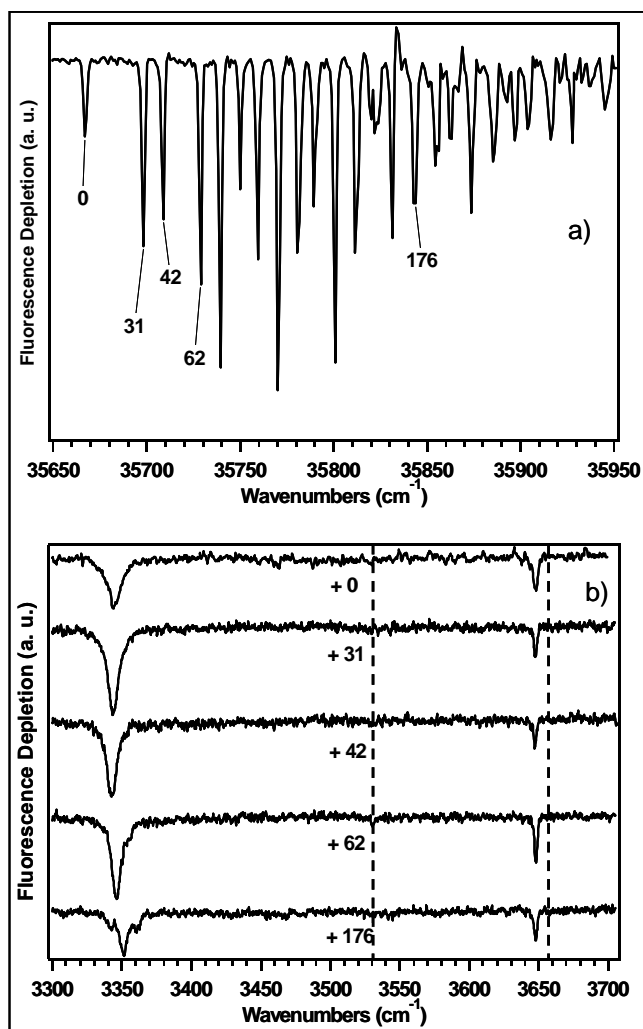


**Figure 9.** a) UVHB spectrum of 2HDPM A with selected transitions labeled to highlight where the excitation takes place for the spectra in b). b) S<sub>1</sub> FDIR spectra of 2HDPM A. The dotted lines indicate the positions of the bound and free OH stretch transitions in the ground state.

The  $S_1$  FDIR spectrum from the 2HDPM B origin provides a striking contrast both with that of 2HDPM A and with its own  $S_0$  FDIR spectrum. As before, a close-up view of the hole-burning spectrum of 2HDPM B is shown in **Figure 10a**), labeled to indicate which excited state vibronic levels serve as starting points for the IR spectra shown in **Figure 10b**). Recall that in the ground electronic state (**Figure 5b**), the OH stretch FDIR spectrum consists of a single peak due to the out-of-phase stretching of the two equivalent OH oscillators (both hydrogen atoms moving in the same direction). If, as suggested by the a/b-hybrid character of the band, the  $S_1$  state retains the  $C_2$  geometry, then the  $S_1$  FDIR spectrum should consist of a single OH stretch fundamental, just as in  $S_0$ . However, the observed spectrum displays a large number of transitions in this region, spread over more than  $100\text{ cm}^{-1}$ . The infrared spectrum of the origin of 2HDPM B contains a weak band at  $3384\text{ cm}^{-1}$  and a strong FC-like progression with a  $\sim 35\text{ cm}^{-1}$  spacing at  $3405$ ,  $3440$ , and  $3472\text{ cm}^{-1}$ . These bands are shifted down from the OH stretch frequency of  $3560\text{ cm}^{-1}$  in  $S_0$ , indicating substantial strengthening of  $\text{OH}\cdots\pi$  H-bonds upon electronic excitation.

The  $S_1$  FDIR spectra out of the  $+22$  and  $+44\text{ cm}^{-1}$  bands are shown below the  $S_1$  origin. A significant change in positions and patterns of levels is seen with increased excitation energy. We will consider the reasons for these unusual spectra in more detail in the discussion section, after considering the SVLF spectra.

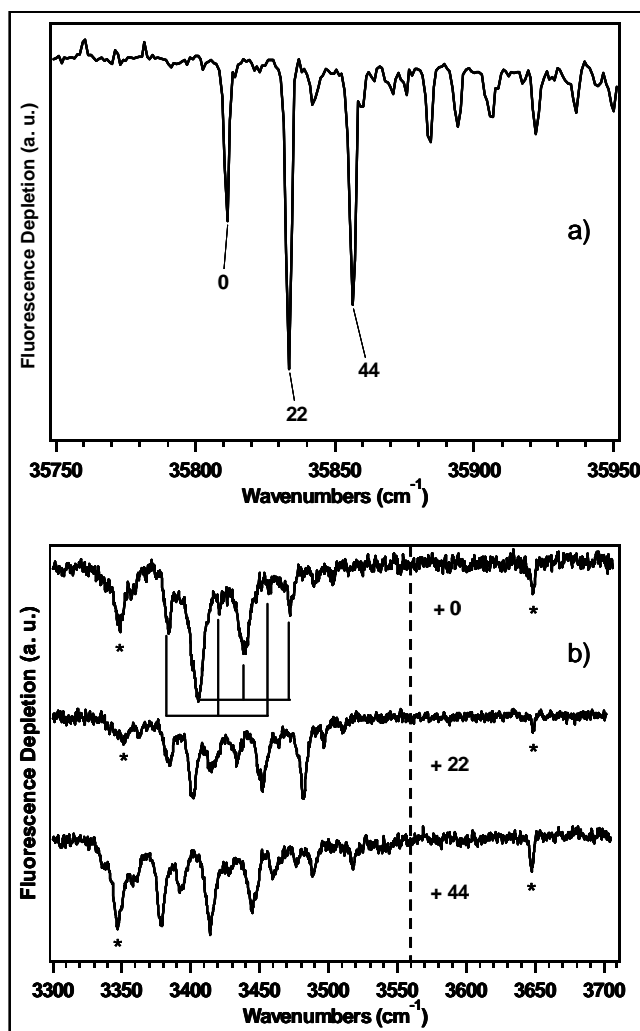


**Figure 10.** a) UVHB spectrum of 2HDPM B with selected transitions labeled to highlight where the excitation takes place for the spectra in b). b)  $S_1$  FDIR spectra of 2HDPM B. The dotted line indicates the position of the single bound OH stretch transition in the ground state. The asterisks mark transitions that arise from small spectral overlap with 2HDPM A when probing 2HDPM B.

#### D. Single Vibronic Level Fluorescence and SEP spectra

##### 1. SVLF Spectra of 2HDPM A

**Figure 11** presents the first  $1100\text{ cm}^{-1}$  of the SVLF spectra of the  $S_1$  origin and the first three vibronic bands of 2HDPM A located  $31$ ,  $42$ , and  $62\text{ cm}^{-1}$  above the origin. The origin spectrum (**Figure 11a**) has long FC progressions which are consistent with the

large geometry change seen in the excitation spectrum. However, unlike the excitation spectrum, which has progressions involving 31 and 42  $\text{cm}^{-1}$  modes, there appears to be a single progression in a 27  $\text{cm}^{-1}$  mode in the SVLF origin spectrum. The +42  $\text{cm}^{-1}$  SVLF spectrum (**Figure 11c**) also has a long FC progression with 27  $\text{cm}^{-1}$  spacing. It shows a bimodal distribution associated with a large displacement in this coordinate. This spectrum has been qualitatively fit using harmonic FC analysis resulting in a D value<sup>51</sup> of 2.3 which is consistent with a large geometry change. As a result, we tentatively associate the 27  $\text{cm}^{-1}$  mode in  $S_0$  with the 42  $\text{cm}^{-1}$  mode in  $S_1$ .

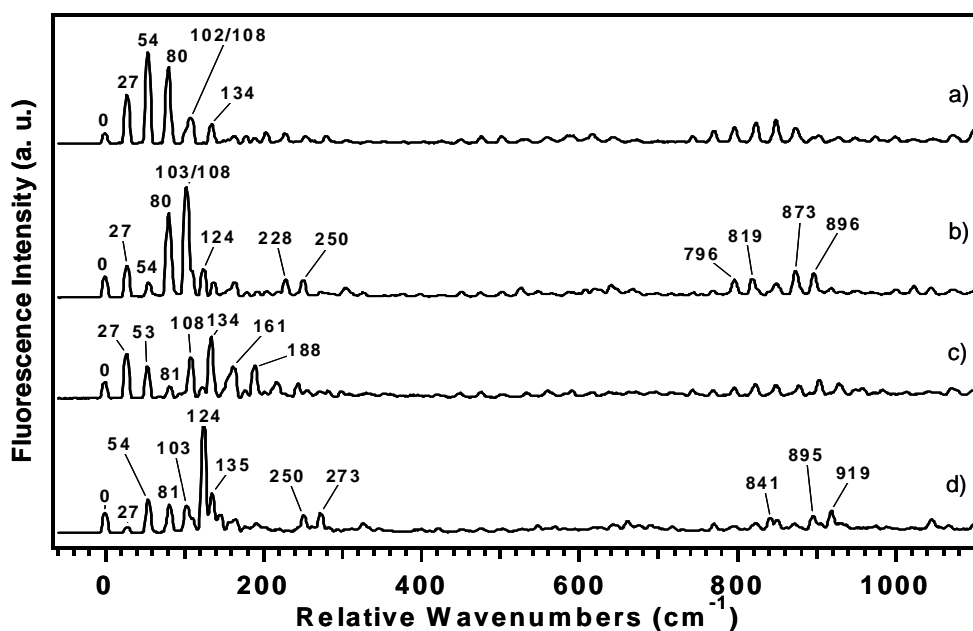


**Figure 11.** SVLF spectra of the 2HDPM A origin (a), +31  $\text{cm}^{-1}$  (b), +42  $\text{cm}^{-1}$  (c), and +62  $\text{cm}^{-1}$  (d) bands.

The SVLF spectrum of the +31  $\text{cm}^{-1}$  band (**Figure 11b**) is highly unusual. The upper state vibronic level responsible for this spectrum ( $T^1$ ) would be expected to support a long progression with changed intensity along T, thereby identifying its vibrational

frequency in the ground state. However, two transitions at +80 and +103  $\text{cm}^{-1}$  dominate the spectrum, serving as false origins for phenol-like transitions built off of them (e.g. +796 and +819  $\text{cm}^{-1}$ ), but without higher members of progressions in either 80 or 103  $\text{cm}^{-1}$  apparent in the spectrum. In the same way, the SVLF spectrum from the transition 62  $\text{cm}^{-1}$  above the origin (**Figure 11d**) shows emission that is dominated by a single false origin at +124  $\text{cm}^{-1}$  with similar phenol-like bands built off of it. The unusual intensities in the +31 and +62  $\text{cm}^{-1}$  SVLF spectra suggest that the low-frequency vibrations of 2HDPM A may engage in extensive Duschinsky mixing, or that vibronic coupling is playing a significant role in dictating these intensities.

## 2. SEP of 2HDPM A

As an aid in making assignments and assessing these possibilities, SEP spectra were recorded. The improved resolution of SEP spectra (2.5  $\text{cm}^{-1}$  versus 8  $\text{cm}^{-1}$  for the SVLF spectra) provides a basis for a more careful search for overlapped transitions in the spectrum.

**Figure 12** shows the low-frequency regions of the SEP spectra for the same set of four transitions of 2HDPM A probed earlier in SVLF. The SEP spectra are shown inverted so that the fluorescence dips associated with SEP dump transitions could be lined up with the SVLF bands above them. Spectra above the  $S_1$  origin have gains in the low-frequency region from dump laser resonances with transitions in the excitation spectrum. The key aspects of these spectra are the following:

- 1) The relative intensities of the anomalous bands in the SEP spectra are faithful replications of the SVLF intensities, indicating that all emission comes from the  $S_1$  state.

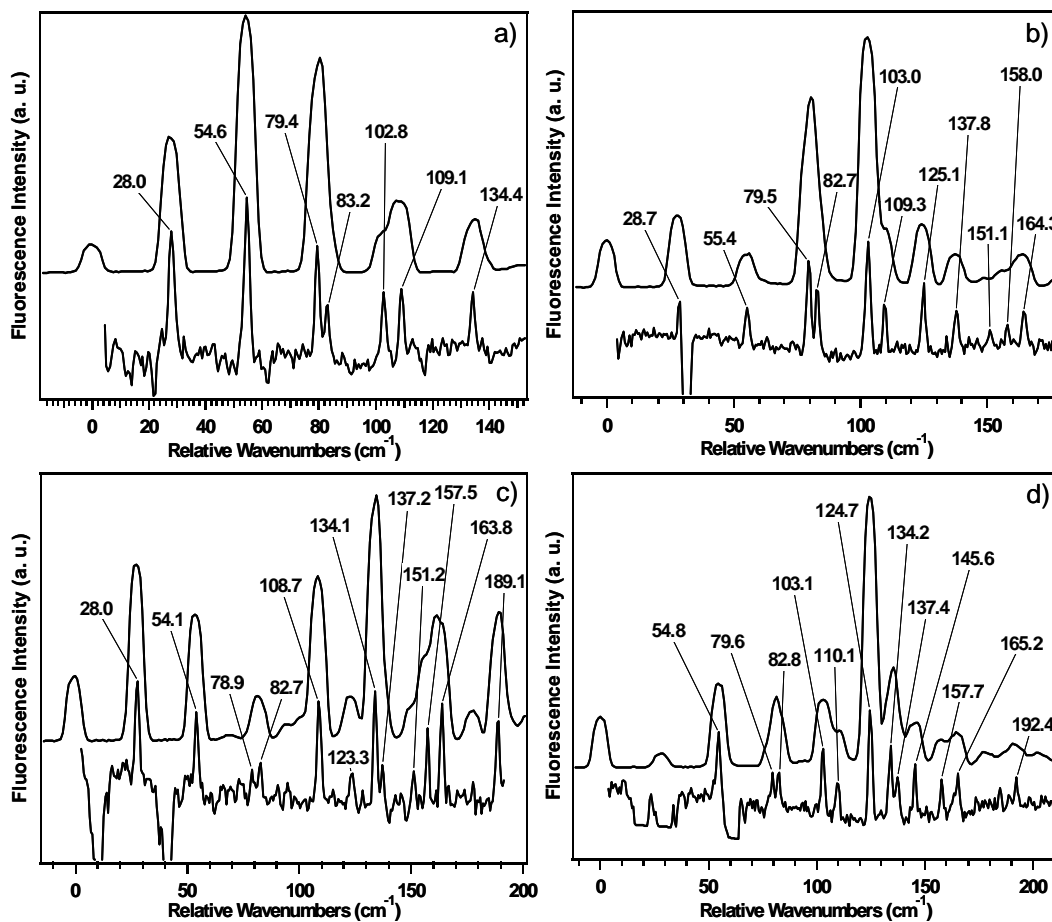


**Figure 12.** SVLF and SEP spectra of 2HDPM A. The SEP spectra (bottom traces) are shown inverted to compare to the SVLF spectra (top traces). The spectra are labeled as follows: a) origin, b) +31, c) +42, d) +62  $\text{cm}^{-1}$ .

- 2) A single, long progression in a 27  $\text{cm}^{-1}$  mode is observed in the  $S_1$  origin SEP scan along with two extra bands at 79 and 103  $\text{cm}^{-1}$  (**Figure 12a**). The 79/83 and 103/109 pairs appear to be in Fermi resonance with one another.
- 3) Most of the long, double-humped set of bands in the spectrum of the +42  $\text{cm}^{-1}$  band (**Figure 12c**) can indeed be interpreted as a single progression in a 27  $\text{cm}^{-1}$  mode. This associates the +42  $\text{cm}^{-1}$  vibration in the excited state most closely with the 27  $\text{cm}^{-1}$  vibration in the ground state.

- 4) The SEP spectrum of the  $+31\text{ cm}^{-1}$  band (**Figure 12b**) has strong transitions at 79 and  $103\text{ cm}^{-1}$ , as surmised by the lower resolution SVLF spectra. In addition, there is a prominent band not fitting the  $27\text{ cm}^{-1}$  progression at  $125\text{ cm}^{-1}$ .
- 5) The spectrum of the  $+62\text{ cm}^{-1}$  band (**Figure 12d**) has as its dominant transition the band at  $125\text{ cm}^{-1}$ , which is surrounded by several other transitions that appear to be Duschinsky or anharmonically mixed with it.

This data can be used to make a set of tentative assignments for the four lowest frequency vibrations to modes with frequencies of 27, 79, 103, and  $125\text{ cm}^{-1}$ . These observed frequencies are to be compared with the calculated low-frequency vibrations at 27 (torsion, T), 55 (butterfly,  $\beta$ ), 104 (anti-symmetric torsion,  $\bar{T}$ ), and  $149\text{ cm}^{-1}$  (out-of-phase butterfly,  $\Omega$ ). We tentatively assign the  $S_0$  fundamentals as  $27=T$ ,  $79=\beta$ ,  $103=\bar{T}$ , and  $125\text{ cm}^{-1}=\Omega$  (see **Table 1**). In making these assignments, we note that the torsions are well reproduced by calculation, but the in-phase and out-of-phase butterfly motions are not. Note that the experimental frequency for the in-phase butterfly  $\beta$  is higher in frequency than calculation by  $24\text{ cm}^{-1}$ , while the out-of-phase butterfly mode is lower in frequency by a similar amount.

The SVLF and SEP spectra show ample evidence for the presence of extensive Duschinsky mixing in 2HDPM A. While the  $+41\text{ cm}^{-1}$  transition is best assigned to  $T^1_0$ , other excited state levels show strong cross-sequence transitions that reflect this mixing. We have not attempted a quantitative Duschinsky analysis, which would need to take into account the rotation and displacement of the normal modes associated with at least four low-frequency vibrations. In addition, the intensities are likely affected by vibronic interactions, a point which is explored further in the Discussion section.

### 3. SVLF of Conformer B

The UVHB spectrum of 2HDPM B (**Figure 4c**) revealed three dominant transitions:  $0^0$ , +22, and +44  $\text{cm}^{-1}$ , suggestive of a progression in a 22  $\text{cm}^{-1}$  vibration.

**Figure 13a)-c)** presents SVLF spectra of the first 1400  $\text{cm}^{-1}$  for these three bands.

Unfortunately, it was not possible to take SEP spectra of these transitions because of the multitude of interfering dump laser resonances with transitions from 2HDPM A.

Therefore, we could not check for overlapped transitions or anomalous intensities in the SVLF spectra.

The origin SVLF spectrum (**Figure 13a**) is dominated by resonance fluorescence and lacks the kind of reflection symmetry one would anticipate if a 22  $\text{cm}^{-1}$  progression in excitation were due to displacement along this normal coordinate. This spectrum also contains a slight background due to overlap with a vibronic band of 2HDPM A, but a careful analysis of a series of spectra taken with the excitation laser fixed at different wavelengths across the band showed that the spectrum of **Figure 13a** is minimally affected by this overlap.

Tentative assignments can be made for several of the observed bands by comparison with the vibrational frequencies obtained from the DFT calculations (**Table 1**). These calculations gave values of 41, 60, and 64  $\text{cm}^{-1}$  for the T,  $\bar{T}$ , and  $\beta$  modes, respectively. The origin SVLF spectrum of 2HDPM B shows several low frequency bands located 37, 62, 101, and 127  $\text{cm}^{-1}$  from the origin transition (**Figure 13a**). We tentatively assign the 37  $\text{cm}^{-1}$  band to  $T^0_1$  and the 62  $\text{cm}^{-1}$  band to  $\beta^0_1$  because they are totally symmetric vibrations which match well with the

calculated frequencies. Given the  $C_2$  symmetry of 2HDPM B in both  $S_0$  and  $S_1$  states, the  $125\text{ cm}^{-1}$  band is assigned to the  $\bar{T}^0_2$  transition involving the first overtone of the non-totally symmetric ('b' symmetry) torsional vibration. On this basis,  $v''=1$  in  $\bar{T}$  would have a frequency of  $125/2$  or  $62.5\text{ cm}^{-1}$ , a close match with the calculated value of  $60\text{ cm}^{-1}$ .

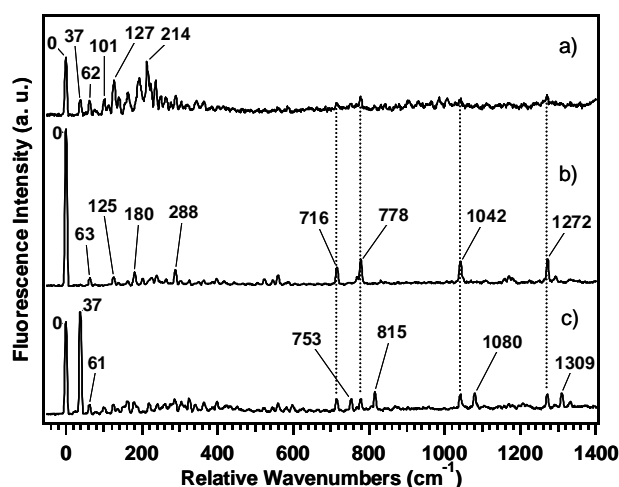


**Figure 13.** SVLF spectra of the 2HDPM B origin (a),  $+22\text{ cm}^{-1}$  (b), and  $+44\text{ cm}^{-1}$  (c) bands.

Surprisingly, resonance fluorescence also dominates the SVLF spectrum of the  $+22\text{ cm}^{-1}$  band (**Figure 13b**) which shows cresol-like vibronic transitions built off of it (e.g.,  $+716$ ,  $+778$ ,  $+1042$ , and  $+1272\text{ cm}^{-1}$ ).<sup>52</sup> It is hard to reconcile this spectrum with an assignment of the  $+22\text{ cm}^{-1}$  transition to  $v''=1$  in a  $22\text{ cm}^{-1}$  mode. The  $+44\text{ cm}^{-1}$  band SVLF spectrum, shown in **Figure 13c**, is also remarkably simple, but very different from expectation. Here, two transitions, one the resonance fluorescence back to the ground state zero-point level, and the other shifted to lower frequency by  $37\text{ cm}^{-1}$ , dominate the spectrum. These anomalies will be discussed further in the discussion section.

## IV. DISCUSSION AND CONCLUSIONS

### A. Ground state conformers and their infrared spectral signatures

2HDPM is a molecule whose torsional motions comprise a 4-dimensional potential energy surface arising from its four flexible coordinates (2 phenyl torsions, 2 OH torsions). Interconversion pathways between possible conformers principally involve these four coordinates. Our spectroscopic investigation has uncovered two distinguishable conformational isomers, one containing an OH $\cdots$ O hydrogen bond (2HDPM A), another containing two OH $\cdots$  $\pi$  hydrogen bonds (2HDPM B).

The rotational constants derived from the high resolution ultraviolet spectra and the characteristics of the conformation-specific infrared spectra provide firm experimental evidence for these two structures. The OH stretch IR spectrum of 2HDPM A reflects formation of a single strong OH $\cdots$ O H-bond and the presence of a free OH stretch, consistent with the calculated structure for this conformer. This inter-ring H-bond locks the two phenyl rings into a Gable-like structure (**Figure 3a**). The rotational constants are consistent with the structure calculated at the B3LYP/6-31+G(d) level of theory, which has both torsional (dihedral) angles between the planes of the two phenol rings and the C(Ph)-CH<sub>2</sub>-C(Ph) plane at about 100°, so that the two rings are in a nearly face-to-face geometry. According to this calculation, the donor OH group is rotated out of the plane of the ring by about 6° in forming the H-bond to the acceptor oxygen (in phenol this bond is in-plane<sup>53</sup>). However, neither the rotational constants nor the OH stretch infrared spectra are sensitive enough to corroborate this structural detail convincingly.

Conversely, the rotational structure and  $S_0$  IR spectra of 2HDPM B provide evidence for a doubly  $\text{OH}\cdots\pi$  H-bonded structure with  $C_2$  symmetry. The structure calculated at the B3LYP/6-31+G(d) level of theory shows that the phenol rings have torsional angles of about  $55^\circ$  with respect to the  $\text{C}(\text{Ph})\text{-CH}_2\text{-C}(\text{Ph})$  plane compared to roughly  $60^\circ$  for DPM<sup>54</sup>. This brings the planes of the two phenyl rings to an angle very near  $90^\circ$ . This calculation also predicts that the two OH groups are tilted out of the plane of their respective aromatic ring by about  $19^\circ$  in reaching toward the  $\pi$  cloud on the opposing ring. The single OH stretch fundamental observed for this doubly  $\text{OH}\cdots\pi$  bound complex is at  $3560\text{ cm}^{-1}$ , within  $30\text{ cm}^{-1}$  of the value of the  $\text{OH}\cdots\text{O}$  hydrogen bonded OH stretch fundamental in 2HDPM A. This reflects the significant strength of these non-traditional  $\text{OH}\cdots\pi$  H-bonds. The similar populations of these two conformers point towards the two conformers possessing similar stabilities, despite the very different mode of inter-ring binding. Direct experimental evidence for their relative stabilities will be provided in the following paper.<sup>21</sup>

## **B. 2HDPM as a flexible bichromophore**

One of the motivations for this work was to gain insight into the electronic coupling between two chromophores connected by a flexible linkage. In this sense, 2HDPM is a close analog of the prototypical flexible bichromophore diphenylmethane (DPM), which we have recently studied in considerable detail.<sup>20</sup> In that case, we were able to identify the  $S_1$  and  $S_2$  origins, which were separated by only  $123\text{ cm}^{-1}$ . The spectroscopic consequences of this close proximity were evident in the high resolution rotational structure and the SVLF spectra, both of which showed evidence for internal

mixing of the  $S_2$  origin with nearby  $S_1$  vibronic levels. By analyzing these spectra, we were able to obtain a state-to-state view of the internal mixing.

In the case of 2HDPM, there are two spectroscopically distinguishable ground-state conformations. In principle, this opens up the opportunity to project onto the two close-lying excited state surfaces from two quite different initial geometries. Our goals included establishing the excited state structures of  $S_1$  and  $S_2$  states, the degree of electronic localization or delocalization, the nature and magnitude of the changes in geometry that accompany electronic excitation, and the nature of the internal mixing between them. We have only been partially successful in addressing these issues, in part because the  $S_1$  rovibronic spectroscopy is so highly unusual. This section gathers together the spectroscopic evidence, the deductions that can be drawn from them, and what remains for further investigation.

### 1. The Excited State Properties of the OH $\cdots$ O Conformer

The OH $\cdots$ O conformer of 2HDPM possesses two distinguishable aromatic rings, one acting as H-bond donor, and the other as acceptor. In this sense, conformer A of 2HDPM is a close analog to the phenol dimer, which also binds via an inter-ring OH $\cdots$ O H-bond. When phenol acts as H-bond donor, it shifts the  $S_0$ - $S_1$  origin to the red by several hundred  $\text{cm}^{-1}$  from that of phenol monomer, while the acceptor ring is blue-shifted.<sup>55</sup> If this splitting is sufficiently large relative to the excitonic coupling, the first two excited states will be localized on the donor and acceptor aromatic rings, respectively.

There is spectroscopic evidence that this localization is present, although it is likely not complete. The  $S_1$  FDIR spectrum of 2HDPM A (**Figure 9b**) shows OH stretch fundamentals ascribable to a H-bonded and a free OH stretch, consistent with retention of this OH $\cdots$ O geometry in the excited state. This is also born out by the high resolution ultraviolet spectrum, which shows modest changes in rotational constants upon electronic excitation. More importantly, in the  $S_1$  state, the H-bonded OH stretch shifts to lower frequency by  $\sim 200\text{ cm}^{-1}$  from its ground state value, indicating that its H-bond to the acceptor oxygen is strengthened by electronic excitation. This is the same effect observed in previous studies of phenol dimer.<sup>47,56</sup> At the same time, the frequency of the free OH stretch on the acceptor ring is essentially unaffected by electronic excitation. Finally, the TDM direction of the  $S_1$  state is oriented close to that of bare cis-o-cresol,<sup>57</sup> when projected onto the phenol ring that acts as the H-bond donor. There is a small rotation of the TDM out of the plane of the ring by about  $10^\circ$  towards the opposing ring. We are thus left with the over-all picture of the  $S_1$  excited state of 2HDPM A as largely localized on the donor ring.

While the extensive low-frequency vibronic structure reminds us of the flexible nature of the 2HDPM bichromophore, there are many aspects of this structure that are as they should be if electronic excitation were completely localized, without significant interaction with a second excited state. First, the low-frequency vibrations are quite harmonic over the entire  $S_1$  Franck-Condon envelope. Second, the excited state rotational constants change with vibrational excitation in the linear fashion expected for vibration-rotation coupling (**Figure 7**), providing confirming evidence for each excited state levels' assigned quantum numbers. Third, neither the direction of the TDM (**Table**

4 and in **Table S1**, supplementary material) nor the  $S_1$  OH stretch fundamentals (**Figure 9a**) change significantly with excitation of the low-frequency vibrations of 2HDPM A, indicating that large-amplitude motions of the two rings do not effect the character of the excited state significantly.

The long Franck-Condon progressions in the excitation spectrum and SVLF spectra reflect the geometry change that accompanies electronic excitation of 2HDPM A. Based on the  $S_1$  origin SVLF spectrum (**Figure 11a**), this geometry change seems to primarily be along the symmetric inter-ring torsion  $T$ , with frequency  $27\text{ cm}^{-1}$  in  $S_0$ . The  $42\text{ cm}^{-1}$  vibration in  $S_1$  appears to correspond sufficiently well to the torsion  $T$  in  $S_0$  ( $27\text{ cm}^{-1}$ ), with the torsional progression  $v'=0,1,2$  in the  $42\text{ cm}^{-1}$  mode being accounted for with a displacement parameter  $D=2.3$ .

Based on its SVLF spectrum (**Figure 11b, 12b**), the  $31\text{ cm}^{-1}$  vibration in  $S_1$  projects onto  $S_0$  as a mixture of asymmetric phenyl torsion  $\bar{T}$  and inter-ring bend  $\beta$ , requiring a Duschinsky analysis including at least these modes. Furthermore, the intensities of progressions involving one low-frequency mode depend on the nature of the vibronic level off of which they are built, sometimes in startling ways. Such differences are responsible for the unusual intensity patterns in the SVLF spectra of the +31 and +62  $\text{cm}^{-1}$  bands (**Figure 11b,d**), which are dominated by strong bands at unexpected positions (80/103 in the former case and  $124\text{ cm}^{-1}$  in the latter). This appearance arises because progressions in  $T$  ( $27\text{ cm}^{-1}$ ) are almost entirely missing built off these levels, despite the fact that such progressions are strong built off of the resonance fluorescence peak. This sensitivity of the symmetric torsion progressions to excitation in  $\bar{T}$  was also present in diphenylmethane.<sup>20</sup> Such effects may result from the large-amplitude nature of the

vibrations, which could enhance intermode coupling. Vibronic effects may also be at work, with modulation of excitonic coupling between  $S_1$  and  $S_2$  with vibrational excitation.

A remaining unanswered question is the location of the second excited state,  $S_2$ , in 2HDPM A. We have already argued for a significant separation of several hundred  $\text{cm}^{-1}$  associated with a red-shift in the donor and a blue-shift in the acceptor ring upon electronic excitation. The UVHB spectrum of **Figure 4b** shows a second set of transitions near  $36200 \text{ cm}^{-1}$  with a different intensity pattern to its low-frequency progressions. These transitions are likely candidates for the  $S_2$  origin, with an  $S_1$ - $S_2$  separation of  $\sim 400\text{-}500 \text{ cm}^{-1}$ . This is to be compared with the  $123 \text{ cm}^{-1}$  separation between  $S_1$  and  $S_2$  in diphenylmethane, with its identical chromophores.

## 2. The Excited State Properties of the $\text{OH}\cdots\pi$ Conformer

Conformer B of 2HDPM is a doubly  $\text{OH}\cdots\pi$  H-bonded conformer. Based on the OH stretch spectrum in the ground state and the direction of the TDM moment of the  $S_0$ - $S_1$  origin transition (82 a: 18 b), we have deduced that both  $S_0$  and  $S_1$  states possess  $C_2$  symmetry. As a result, the  $S_1$  and  $S_2$  states should form an excitonic pair in which the electronic excitation is delocalized over both rings, in this case with the (presumably)  $S_1$  state of B symmetry, as it is in DPM.

The excitation spectrum of 2HDPM B is dominated by three vibronic transitions with spacing of  $22 \text{ cm}^{-1}$ , seemingly forming a vibronic progression in a  $22 \text{ cm}^{-1}$  excited state mode. All three bands are a:b hybrids, in keeping with their assignment to a vibrational progression. As a result, we have not been able to locate the  $S_2$  state, which

should be a pure 'c'-type band. Furthermore, the vibronic spectroscopy of 2HDPM B contains many highly unusual aspects that arise from the presence of strong vibronic effects which signal the close presence of, and close interaction with, the  $S_2$  state. First, there is a striking lack of symmetry between the fluorescence excitation spectrum (with the alleged progression in the  $22\text{ cm}^{-1}$  vibration) and the  $S_1$  origin SVLF spectrum (with strong  $\Delta v=0$  FC factors). Second, the TDM direction undergoes changes in the  $44\text{ cm}^{-1}$  vibronic progression that are unusually large, swinging from 82 a:18 b at the  $S_1$  origin and 79 a:21 b in the  $+22\text{ cm}^{-1}$  band to 91 a:9 b in the  $+44\text{ cm}^{-1}$  band. However, all three must gain oscillator strength from  $S_1$ , since all retain a strong 'a' component to their band character. Third, the SVLF spectra of 0,  $+22$ , and  $+44\text{ cm}^{-1}$  transitions (**Figure 13**) show intensity patterns that cannot be accounted for by any harmonic, dipole-allowed set of transitions involving a progression in a symmetric vibration of frequency  $22\text{ cm}^{-1}$ . The strong resonance fluorescence from the  $+22\text{ cm}^{-1}$  level is particularly puzzling in this regard.

All these unusual aspects of the vibronic spectroscopy, particularly the SVLF intensity patterns, seem to be characteristic features of these flexible bichromophores. In 2HDPM and DPM (both of which have two identical UV chromophores), the unusual intensity patterns can arise from the close proximity of the two excited states, which could make the magnitude and direction of the TDM extraordinarily sensitive to vibrational excitation. On the other hand, even if the two chromophores are not identical, the large-amplitude motion of the torsional and bending vibrations changes the distance and orientation of the two rings to a larger extent than in rigid molecules, and could swing the TDM direction and magnitude by virtue of this large-amplitude motion. In the

present study, we cannot clearly distinguish between these two possibilities, calling for future studies that involve a series of flexible bichromophores with differing electronic energy separations.

A full explanation of these couplings requires a knowledge of the excited state surfaces which extends far beyond simple optimizations of the  $S_1$  and  $S_2$  minima, but instead encompasses whole regions of the torsional and inter-ring bending excited state surfaces about the minima. In particular, understanding the unusual intensity patterns in the SVLF spectra may require mapping out the transition dipole moment surface of the  $S_1$  and  $S_2$  states from  $S_0$ . It seems likely to us that the transition moment magnitude and direction will be a sensitive function of the phenyl ring torsion, OH torsion, and inter-ring bending angles. This is particularly the case in 2HDPM B because its inter-ring angle at equilibrium is very near 90 degrees, which may result in an unusual sensitivity of the direction and magnitude of the TDM's of the  $S_1$  and  $S_2$  states to inter-ring torsion and bending excitation. As a result, the intensity of a vibronic band connecting a given pair of  $S_0$  and  $S_1$  vibronic levels can only be quantitatively accounted for by computing the wave functions and dipole moment over the full range of geometries sampled by the ground and excited state vibrational wave functions, and then computing the transition moment integral over this surface. A full account of such issues thus awaits theoretical modeling of the excited state surfaces at a sufficient level of detail and accuracy.

Even the OH stretch infrared spectra of 2HDPM B, which are anticipated to involve vibrational excitation within a single (excited) electronic state, show dramatic changes associated with electronic excitation. The  $S_1$  FDIR spectra coming out of the 0, +22, and +44  $\text{cm}^{-1}$  upper levels (**Figure 10**), which are anticipated to have a single

allowed OH stretch fundamental (as in  $S_0$ ), exhibit an complicated progression of bands with intensity spread over almost  $150\text{ cm}^{-1}$ . The dominant sub-structure is composed of two triads of peaks, split by  $22\text{ cm}^{-1}$ , with a spacing of  $\sim 35\text{ cm}^{-1}$  in the triad. This pattern shifts and fragments further as the lower level out of which infrared excitation occurs changes from the  $S_1$  origin to  $+22$  and  $+44\text{ cm}^{-1}$ . If these intensity patterns are indeed due to combination bands between the OH stretch and a low-frequency  $S_1$  mode of  $35\text{ cm}^{-1}$ , the inter-mode coupling that gives rise to these combination bands must be strong. Since the ring torsional levels modulate the inter-ring distance, strong coupling between them and the OH stretch modes seems plausible in the doubly OH $\cdots\pi$  H-bonded structure of conformer B. We hypothesize that this  $35\text{ cm}^{-1}$  vibration could be the antisymmetric ring torsion  $\bar{T}$ , and that combination bands involving this mode could asymmetrize the two rings and turn on intensity in both the symmetric and antisymmetric OH stretch modes.

Finally, despite the near proximity of  $S_1$  and  $S_2$  states, no definite assignment for the  $S_2$  origin is in hand, and hence the  $S_1$ - $S_2$  excitonic splitting is not yet determined. Future searches would benefit from state-of-the-art calculations on the excited states in order to guide its experimental detection.

## V. ACKNOWLEDGEMENTS

This work was supported by the Department of Energy Basic Energy Sciences, Division of Chemical Sciences under Grant No. DE-FG02-96ER14656. The authors gratefully acknowledge W. Leo Meerts for his help with the integration of rotational axis reorientation into the Genetic Algorithm. D. F. P. would like to express thanks to Kevin O. Douglass for providing us with the MW data. N. R. P. acknowledges Purdue

University and the Andrews family for the Frederick N. Andrews Fellowship. C. W. M. would like to thank the “Deutsche Akademie der Naturforscher Leopoldina” for a postdoctoral scholarship (grant number BMBF-LPD 9901/8-159 of the “Bundesministerium für Bildung und Forschung”).

## VI. REFERENCES

- (1) LeGreve, T. A.; Clarkson, J. R.; Zwier, T. S. *J. Phys. Chem. A* 2008, *112*, 3911.
- (2) Baquero, E. E.; James III, W. H.; Shubert, V. A.; Zwier, T. S. *J. Phys. Chem. A* 2008, *in press*.
- (3) Borst, D. R.; Joireman, P. W.; Pratt, D. W.; Robertson, E. G.; Simons, J. P. *J. Chem. Phys.* 2002, *116*, 7057.
- (4) Emery, R.; Macleod, N. A.; Snoek, L. C.; Simons, J. P. *PCCP* 2004, *6*, 2816.
- (5) Mons, M.; PiuZZi, F.; Dimicoli, I. *Actualite Chimique* 2007, *314*, 19.
- (6) Selby, T. M.; Zwier, T. S. *J. Phys. Chem. A* 2005, *109*, 8487.
- (7) Snoek, L. C.; Kroemer, R. T.; Hockridge, M. R.; Simons, J. P. *PCCP* 2001, *3*, 1819.
- (8) Chin, W.; PiuZZi, F.; Dimicoli, I.; Mons, M. *PCCP* 2006, *8*, 1033.
- (9) Carcabal, P.; Hunig, I.; Gamblin, D. P.; Liu, B.; Jockusch, R. A.; Kroemer, R. T.; Snoek, L. C.; Fairbanks, A. J.; Davis, B. G.; Simons, J. P. *J. Am. Chem. Soc.* 2006, *128*, 1976.
- (10) Macleod, N. A.; Simons, J. P. *PCCP* 2004, *6*, 2821.
- (11) Simons, J. P.; Jockusch, R. A.; Carcabal, P.; Hung, I.; Kroemer, R. T.; Macleod, N. A.; Snoek, L. C. *Int. Rev. Phys. Chem.* 2005, *24*, 489.
- (12) de Vries, M. S.; Hobza, P. *Annu. Rev. Phys. Chem.* 2007, *58*, 585.
- (13) Clarkson, J. R.; Dian, B. C.; Moriggi, L.; DeFusco, A.; McCarthy, V.; Jordan, K. D.; Zwier, T. S. *J. Chem. Phys.* 2005, *122*.
- (14) Pillsbury, N. R.; Zwier, T. S. *J. Phys. Chem. A* 2008, *accepted*.

- (15) Selby, T. M.; Clarkson, J. R.; Mitchell, D.; Fitzpatrick, J. A. J.; Lee, H. D.; Pratt, D. W.; Zwier, T. S. *J. Phys. Chem. A* 2005, *109*, 4484.
- (16) Selby, T. M.; Zwier, T. S. *J. Phys. Chem. A* 2007, *111*, 3710.
- (17) LeGreve, T. A.; Clarkson, J. R.; Zwier, T. S. *J. Phys. Chem. A* 2008, *112*, 3911.
- (18) Shubert, V. A.; Baquero, E.; Clarkson, J. R.; James III, W. H.; Turk, J. A.; Hare, A. A.; Worrel, K.; Lipton, M. A.; Schofield, D. P.; Jordan, K. D.; Zwier, T. S. *J. Chem. Phys.* 2007, *127*, 234315.
- (19) Pillsbury, N. R.; Stearns, J. A.; Douglass, K. O.; Müller, C. W.; Zwier, T. S.; Plusquellic, D. F. *J. Chem. Phys.* 2008, (*accepted*).
- (20) Pillsbury, N. R.; Stearns, J. A.; Müller, C. W.; Plusquellic, D. F.; Zwier, T. S. *J. Chem. Phys.* 2008, *accepted*.
- (21) Pillsbury, N. R.; Zwier, T. S. *adjoining paper* 2008.
- (22) Katsyuba, S.; Chernova, A.; Schmutzler, R.; Grunenberg, J. *Journal of the Chemical Society-Perkin Transactions 2* 2002, 67.
- (23) Majewski, W.; Meerts, W. L. *J. Mol. Spec.* 1984, *104*, 271.
- (24) Majewski, W. A.; Plusquellic, D. F.; Pratt, D. W. *J. Chem. Phys.* 1989, *90*, 1362.
- (25) Plusquellic, D. F.; Davis, S. R.; Jahanmir, F. *J. Chem. Phys.* 2001, *115*, 225.
- (26) Zwier, T. S. *J. Phys. Chem. A* 2006, *110*, 4133.
- (27) Jusinski, L. E.; Taatjes, C. A. *Rev. Sci. Instr.* 2001, *72*, 2837.
- (28) Plusquellic, D. F.; Lavrich, R. J.; Petralli-Mallow, T.; Davis, S.; Korter, T. M.; Suenram, R. D. *Chem. Phys.* 2002, *283*, 355.
- (29) Riedle, E.; Ashworth, S. H.; Farrell, J. T.; Nesbitt, D. J. *Rev. Sci. Instr.* 1994, *65*, 42.

- (30) Hageman, J. A.; Wehrens, R.; de Gelder, R.; Meerts, W. L.; Buydens, L. M. C. *J. Chem. Phys.* 2000, *113*, 7955.
- (31) Meerts, W. L.; Schmitt, M.; Groenenboom, G. C. *Can. J. Chem.* 2004, *82*, 804.
- (32) Plusquellic, D. F.; Suenram, R. D.; Mate, B.; Jensen, J. O.; Samuels, A. C. *J. Chem. Phys.* 2001, *115*, 3057.
- (33) Majewski, W. A. P., J. F.; Plusquellic, D. F.; Pratt, D. W. in: A. B. Myers and T. R. Rizzo (Eds.) *Laser Techniques in Chemistry*; Wiley: New York, 1995; Vol. XXIII.
- (34) Berden, G.; Meerts, W. L.; Jalviste, E. *J. Chem. Phys.* 1995, *103*, 9596.
- (35) Wu, Y. R.; Levy, D. H. *J. Chem. Phys.* 1989, *91*, 5278.
- (36) Becke, A. D. *Phys. Rev. A* 1988, *38*, 3098.
- (37) Lee, C. T.; Yang, W. T.; Parr, R. G. *Phys. Rev. B* 1988, *37*, 785.
- (38) Frisch, M. J.; Head-Gordon, M.; Pople, J. A. *Chem. Phys. Lett.* 1990, *166*, 281.
- (39) Frisch, M. J.; Trucks, G. W.; Schlegel, H. B.; Scuseria, G. E.; Robb, M. A.; Cheeseman, J. R.; Montgomery, J. A., Jr., T. V.; Kudin, K. N.; Burant, J. C.; Millam, J. M.; Iyengar, S. S.; Tomasi, J.; Barone, V.; Mennucci, B.; Cossi, M.; Scalmani, G.; Rega, N.; Petersson, G. A.; Nakatsuji, H.; Hada, M.; Ehara, M.; Toyota, K.; Fukuda, R.; Hasegawa, J.; Ishida, M.; Nakajima, T.; Honda, Y.; Kitao, O.; Nakai, H.; Klene, M.; Li, X.; Knox, J. E.; Hratchian, H. P.; Cross, J. B.; Bakken, V.; Adamo, C.; Jaramillo, J.; Gomperts, R.; Stratmann, R. E.; Yazyev, O.; Austin, A. J.; Cammi, R.; Pomelli, C.; Ochterski, J. W.; Ayala, P. Y.; Morokuma, K.; Voth, G. A.; Salvador, P.; Dannenberg, J. J.; Zakrzewski, V. G.; Dapprich, S.; Daniels, A. D.; Strain, M. C.; Farkas, O.; Malick, D. K.; Rabuck, A. D.; Raghavachari, K.; Foresman, J. B.; Ortiz, J. V.; Cui, Q.; Baboul, A. G.; Clifford, S.; Cioslowski, J.; Stefanov, B. B.; Liu, G.; Liashenko, A.; Piskorz, P.;

Komaromi, I.; Martin, R. L.; Fox, D. J.; Keith, T.; Al-Laham, M. A.; Peng, C. Y.; Nanayakkara, A.; Challacombe, M.; Gill, P. M. W.; Johnson, B.; Chen, W.; Wong, M. W.; Gonzalez, C.; Pople, J. A. Gaussian 03, Revision E.01; Gaussian, Inc.: Wallingford CT, 2004.

- (40) Head-Gordon, M.; Head-Gordon, T. *Chem. Phys. Lett.* 1994, 220, 122.
- (41) Head-Gordon, M.; Pople, J. A.; Frisch, M. J. *Chem. Phys. Lett.* 1988, 153, 503.
- (42) Møller, C.; Plesset, M. S. *Phys. Rev.* 1934, 46, 0618.
- (43) Sæbø, S.; Almløf, J. *Chem. Phys. Lett.* 1989, 154, 83.
- (44) Foresman, J. B.; Head-Gordon, M.; Pople, J. A.; Frisch, M. J. *J. Phys. Chem.* 1992, 96, 135.
- (45) Aota, T.; Ebata, T.; Ito, M. *J. Phys. Chem.* 1989, 93, 3519.
- (46) Appel, I.; Kleinermanns, K. *Ber. Bunsen Ges. Phys. Chem.* 1987, 91, 140.
- (47) Ebata, T.; Watanabe, T.; Mikami, N. *J. Phys. Chem.* 1995, 99, 5761.
- (48) Wu, Y. R.; Levy, D. H. *J. Chem. Phys.* 1989, 91, 5278.
- (49) Papoušek, D.; Aliev, M. R. *Molecular vibrational-rotational spectra*; Elsevier: Amsterdam, 1982; Vol. Chap. 17.
- (50) Clabo Jr., D. A.; Allen, W. D.; Remington, R. B.; Yamaguchi, Y.; Schaefer III, H. F. *Chem. Phys.* 1988, 123, 187.
- (51) Henderson, J. R.; Muramoto, M.; Willett, R. A. *J. Chem. Phys.* 1964, 41, 580.
- (52) Roth, W.; Imhof, P.; Gerhards, M.; Schumm, S.; Kleinermanns, K. *Chem. Phys.* 2000, 252, 247.
- (53) Larsen, N. W. *J. Mol. Struct.* 1979, 51, 175.
- (54) Feigel, M. J. *J. Mol. Struct.* 1996, 366, 83.

- (55) Fuke, K.; Kaya, K. *Chem. Phys. Lett.* 1983, 94, 97.
- (56) Döpfer, O.; Lembach, G.; Wright, T. G.; Müller-Dethlefs, K. *J. Chem. Phys.* 1993, 98, 1933.
- (57) Myszkiewicz, G.; Meerts, W. L.; Ratzner, C.; Schmitt, M. *PCCP* 2005, 7, 2142.